Code 256

INTERFEROMETER POSITION LOCATION CONCEPT
Phase Recovery and Calibration

Contract No.: NAS5-21043

Federal Systems Division
International Business Machines Corporation
18100 Frederick Pike
Gaithersburg, Maryland 20760

October 1970
Final Report (Phase II)

Prepared for
GODDARD SPACE FLIGHT CENTER
Greenbelt, Maryland 20771

1 Report No	2 Government Accession No	3. Recipient's Catalog No
4 Title and Subtitle INTERFEROMETER POSITION LOCATION CONCEPT Phase Recovery and Calibration		5 Report Date October 1970 6 Performing Organization Code
7 Author(s)		8 Performing Organization Report No FSC-70-5269
9. Performing Organization Name and Address International Business Machines Corp. Federal Systems Division 18100 Frederick Pike Gaithersburg, Md. 20760		10 Work Unit No. 11 Contract or Grant No NAS5-21043 13 Type of Report and Period Covered Final Report (Phase II)
12 Sponsoring Agency Name and Address Goddard Space Flight Center Greenbelt, Maryland 20771 Technical Monitor: F. X. Downey 750		14 Sponsoring Agency Code
15. Supplementary Notes		

17 Key Words (Selected by Author(s))	18 Distribution Statement		
Position Location Interferometer			
19 Security Classif (of this report) Unclassified	20 Security Classif (of this page)	21. No of Pages	22 Price*

*For sale by the Clearinghouse for Federal Scientific and Technical Information, Springfield, Virginia 22151

PREFACE

The objective of this second part of a two-part study was to continue the investigation of the feasibility of locating 15,000 super-pressure-constant altitude balloons by means of spaceborne interferometers in synchronous orbits. The scope of this phase of the program was to study phase recovery and calibration techniques in order to verify the assumptions on which the system concept is based.

The conclusions of this study, based on experimental investigations, are that instrumentation errors in phase recovery can be kept to 0.2 electrical degree (3sigma). Total effective instrumentation errors of 0.9 degree (3 sigma), on which system performance is based, appear feasible because of the negligible effect of phase biases on position location.

It is concluded, as a result of calibration and space angle measurement experiments performed using the ATS F&G breadboard interferometer (26.6 wavelengths), that space angle measurements can be made with a 400-wavelength interferometer to the required accuracy to achieve a position location accuracy of 1 km (1 sigma).

FOREWORD

This report covers the second phase of the work performed on Contract NAS5-21043. Work performed on the first phase was reported in Interferometer Position Location Concept, Final Report, June 1970.

This work was performed at the Federal Systems Center of IBM. Mr. J. E. Henrich and Mr. D. P. Bedford performed the analysis of the calibration experiments. Mr. B. W. Driggs designed the analog circuitry while Mr. F. L. Marek designed the digital. The experiments were performed primarily by Mr. M. A. Teichman and Mr. A. K. Parr. Dr. C. T. Tsitsera was project manager.

The study team received valuable assistance and guidance from Mr. F. X. Downey, technical officer for Goddard Space Flight Center. Mr. M. S. Maxwell, also of GSFC, contributed significantly to the technical content.

CONTENTS

ILLUSTRATIONS

TABLES

Section 1

INTRODUCTION

This report is the second of a two-part study to investigate the feasibility of locating low power emitters at known altitudes by means of an interferometer in synchronous orbit. The results of the first phase of the study made under this contract were presented in a final report[1] which shall be referred to herein as Final Report (Phase I). In that work, the basic system concept was developed. In the portion of the contract covered by this report, concentration was directed to the following:

Phase recovery techniques
Calibration technique.

The interferometry application considered is the location of randomly transmitting weather balloons for the primary purpose of determining average wind velocity through successive position determinations. Super pressure balloons are used which tend to drift at constant altitude.[2] Data transmitted by the balloon include identification number, pressure, and temperature. The system concept is shown in Figure 1-1, and the major system parameters are given in Table 1-1.

Four widely spaced calibration transmitters continually illuminate the satellite. This allows calibration of the baselines, i.e., determination of baseline lengths, orientations, and system phase biases. Baseline motion during phase measurement of balloon signals (10 seconds) is compensated by using the continuously available calibration data.

The beacon horizontal position CEP (circular error probable) achievable by the system is shown in Figure 1-2. Multipath error (not included in Figure 1-2)

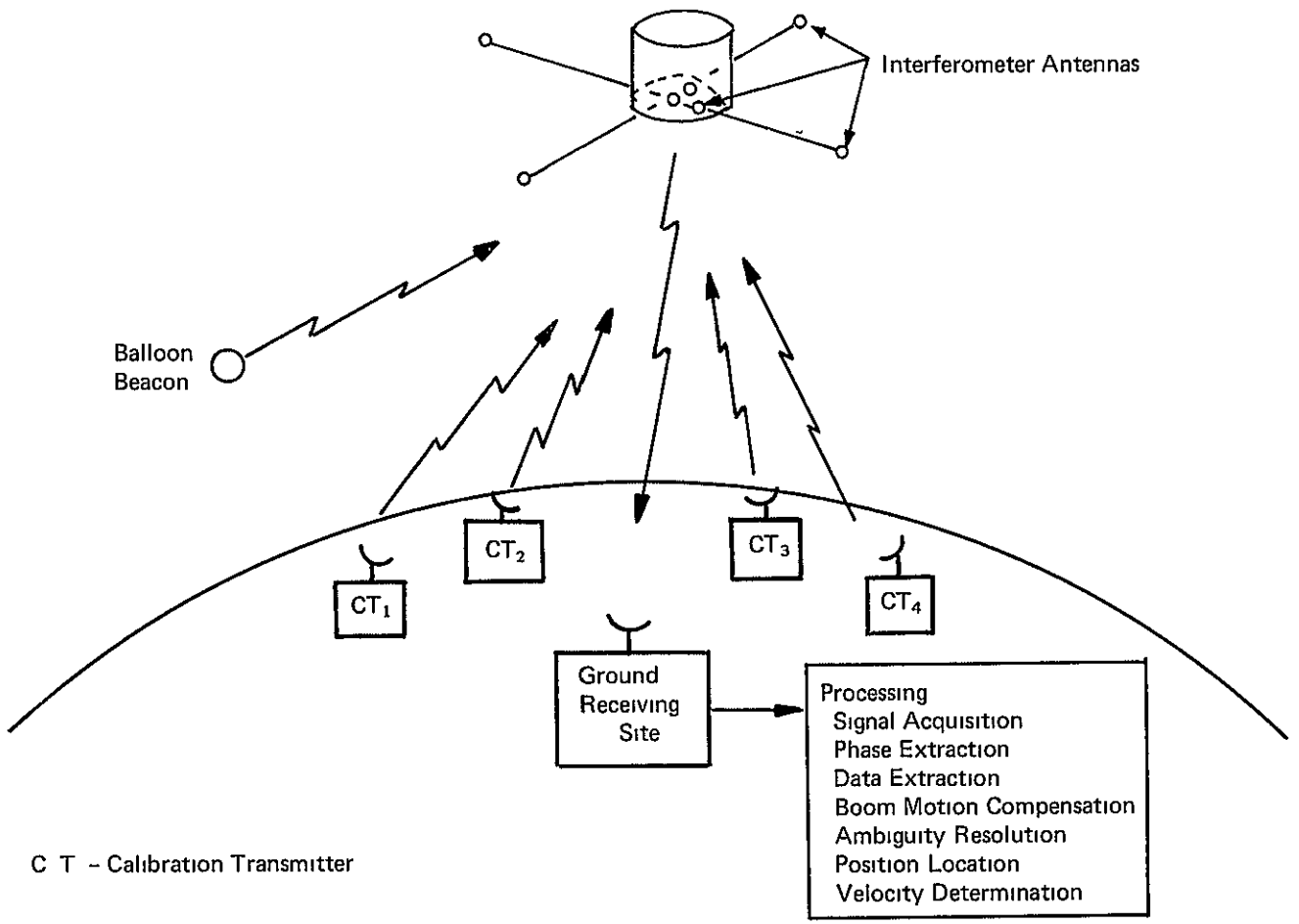

Figure 1-1. System Concept

Table 1-1

SYSTEM PARAMETERS

Operating Frequency (Uplink)	1600 MHz (nominal)
Uplink Bandwidth	30 kHz
Baselines (Vernier)	2 Orthogonal; 75 m 400 wavelengths (400 λ)
Ambiguity-Resolving Baselines	3 λ, 190 λ, 400λ (physical) 20 λ (differential)
Interferometer Antennas (seven required)	Short Backfire 22^{o} half power beamwidth
Polarization	Circular for all antennas
Access Technique	Random (in frequency and time)
Balloon	
Beacon Power	1 W
Oscillator Stability	1 part in 10^{5}
Transmission Time	10 seconds every 2 hours
Data Modulation	Biphase
Data Rate	9 bits per second
Calibration Transmitter	
Number	4
ERP	20 dBW
Transmission Time	Continuous
Phase Measurement Accuracies*(1σ)	
For Beacons	0.6^{o} to 0.9^{o} depending on elevation angle
For Calibration Transmitters	0.45^{o}

*Including instrumentation error of 0.3^{o} (1σ) for each

is a function of beacon altitude as well as elevation angle. Directly under the interferometer or at zero altitude there will be no multipath error. Above elevation angles of 20°, the error will be less than 1 km under most conditions.

The position errors shown in Figure 1-2 are based on measuring phase to an accuracy (1 sigma) of 0.45° for the calibration transmitters and from 0.6° to 0.9° (depending upon elevation angle) for the balloon beacons. These phase errors include instrumentation error components of 0.3° (1 sigma). Errors in phase due to thermal noise are amenable to analysis. Instrumentation errors are less susceptible to prediction, and experimental verification is desirable.

Because of the low ERP (effective radiated power) of the beacons, phase measurements depend upon use of phase-locked loops for signal acquisition, narrow-band filtering in a phase recovery circuit and, finally, phase measurement. The necessity of narrow-band filtering makes the phase recovery operation the most critical as far as instrumentation errors are concerned. It is for this reason that one of the main emphases of this study was phase recovery, and experiments were performed to verify the assumptions and analysis made.

For further investigations of calibration techniques undertaken in this portion of the contract, it was fortunate to have available for experiments the ATS F&G breadboard interferometer.[3,4,5] This interferometer (26.6 wavelengths at 8.15 GHz) was designed for attitude sensing. By appropriately designed experiments performed in an anechoic chamber, this interferometer was used to verify calibration techniques to determine baseline length and also to measure space angles.

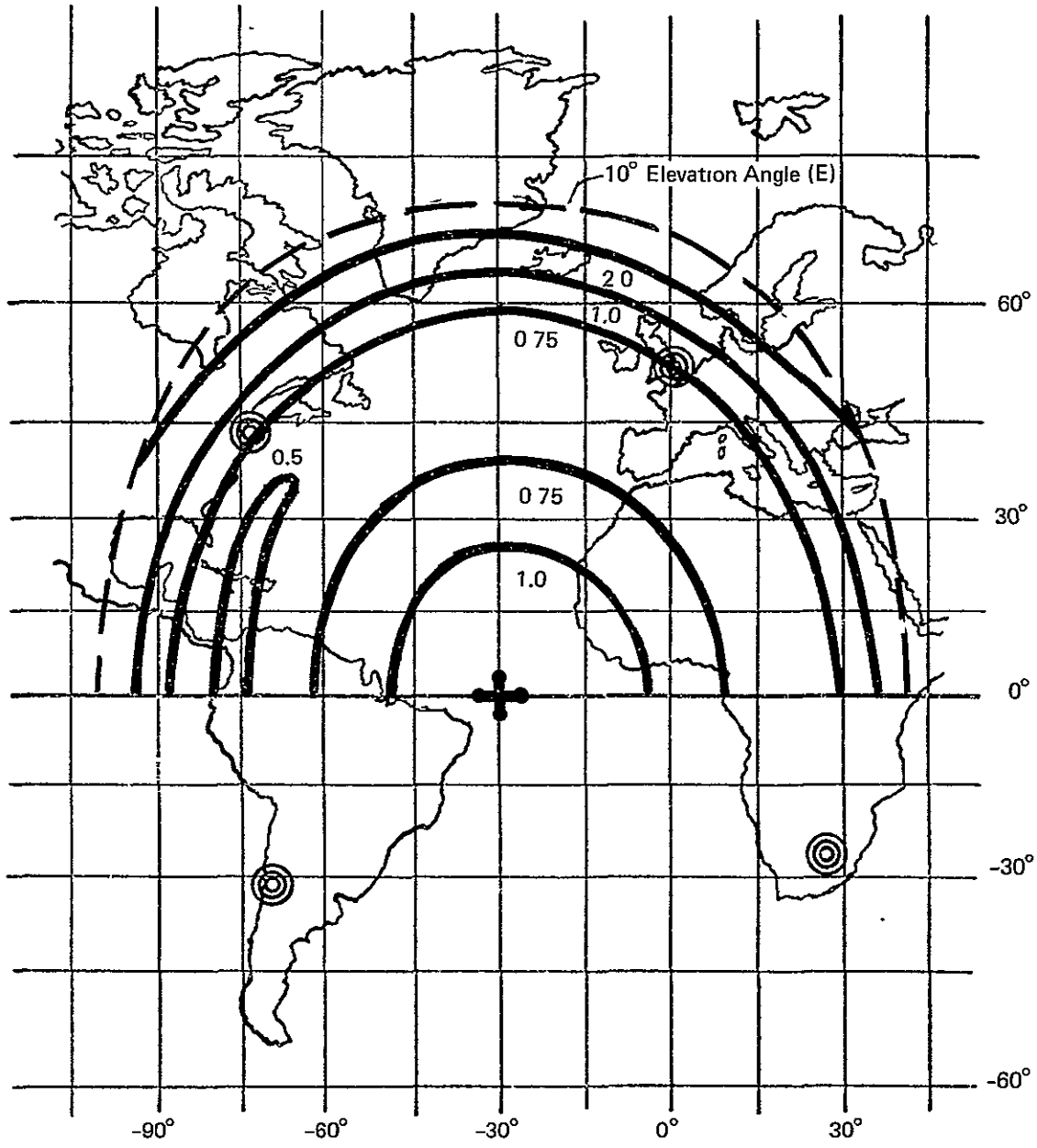

Assumptions:

Calibration Transmitters (CTs)	1 σ Errors
Rosman	CT Noise 0.45°
Santiago	CT Survey (La, Lo, h) 10, 10, 3 m
London	Satellite Ephemeris (N, T, R) 60, 60, 10 m
Johannesburg	Altitude 100 m
	Beacon Noise 0.6° @ E = 90°
	0.9° @ E = 20°

Figure 1-2. Beacon Horizontal Position CEP in km (Multipath Excluded)

Section 2

SUMMARY AND CONCLUSIONS

Phase biases in an interferometer system used for position location are two or three orders of magnitude less important than random phase errors of the same magnitude. Phase biases are defined as consistent phase errors (over a measuring time interval) which are common to both calibration and beacon signal phase measurements. Because of this property of phase biases, it was concluded that potentially the most significant instrumentation errors are in the phase recovery circuits.

A phase recovery circuit was designed and built. The input signals were at 1.1 and 3.1 kHz (separated by a 2 kHz reference). The output of the recovery circuit was two 1.1 kHz signals which contain the desired phase information. Filtering was accomplished by 2-pole, 60 Hz active filters. Circuit tests produced the following results:

1. Peak-to-peak phase deviations over a 75-minute period were 0.2 degrees (equivalent to about 0.1 degrees, 3 sigma). These tests were in a laboratory environment without special temperature control.
2. Phase change with temperature of the circuit was 0.2 degree per degree centigrade.
3. With reference oscillator stability in the satellite and on the ground of 1 part in 10^6, negligible phase error would result from the circuit (less than 0.01 degree).
4. A phase change of 0.2 degree occurred for a 10 dB change in signal levels. A simple automatic gain control circuit would extend the dynamic range.
5. An interfering signal of 0 dB with respect to signal level produced less than 0.3 degree phase error if separated from either of the input signals by more than 25 Hz.

A phase-locked loop was also built. This allowed the circuit to be tested with the ATS F&G breadboard interferometer. The phase deviations of the entire system over a 75-minute period was 0.4 degree peak to peak (approximately 0.2 degree, 3 sigma). This stability is well within the allocated 0.9 degree, 3 sigma, for instrumentation error.

The ATS F&G breadboard interferometer was used to perform calibration and space-angle measurement experiments. A second horn was added in the anechoic chamber so that the interferometer could be illuminated from two positions separated by 5.66° space angle. Phase measurements were made as a function of the interferometer angular position over a space-angle range of 15 degrees (every 0.1 degree of space). A computer program was written to facilitate data processing.

With the assumption that the positions of the two illuminators are known, the data can be used in a calibration mode to determine baseline length and orientation. With the assumption that the position of only one transmitter is known (and the baseline length), the angle between the transmitters can be determined, thus locating the second transmitter. The results of the tests are summarized below:

1. The relative angle between the two illuminators was measured to an accuracy of 0.003 degree (1 sigma), with the orientation of the interferometer varied over 15 degrees.
2. The accuracy of the relative angle measurement between the two illuminators is much less sensitive to phase bias errors than to random errors of the same magnitude. An 80° electrical phase bias changed the estimated orientation of the baseline by as much as 0.44 degree, while the error in relative angle measurement due to the same cause was less than 0.0044 degree.
3. The length of the baseline was estimated with a 1 sigma error of 0.6 mm with the orientation of the interferometer varied over 15 degrees.

Some additional tradeoff analyses were made, including:

1. Effect of boom length (and resulting boom twisting and reduced antenna gain) upon position location accuracy
2. Minimizing dc power in balloon with respect to frequency for given position location error when instrumentation and thermal noise errors predominate.

The following major conclusions can be drawn as a result of work performed in this phase of the contract:

1. Instrumentation errors due to phase recovery circuits can be kept to approximately 0.1° (1 sigma).
2. The performance characteristics as given in the Final Report (Phase I) and summarized in Figure 1-2, which were based on an instrumentation error of 0.3° (1 sigma), are reasonable.
3. The calibration experiment results of relative angle measurement of 0.003 degree (1 sigma) with a 26.6-wavelength interferometer translate to 0.0002 degree (1 sigma) with a 400-wavelength interferometer. This is equivalent to a position location error of 0.2 km from synchronous altitude. These results, therefore, indicate high confidence in meeting a 1 km (1 sigma) position location accuracy.

Section 3

RECOMMENDATIONS

Studies and experiments performed to date have indicated that the interferometer position location concept is feasible. It is recommended, therefore, that work in this area continue. The following three-step program culminating in a flight experiment is suggested:

1. Boom Development and Testing—The most promising boom designs should be tested in a thermal vacuum chamber for thermal bending and thermal twisting; a boom package should be developed, including deployment mechanism for the coaxial cable; and dynamic analysis of booms and interaction with spacecraft should be continued.
2. Experiment Development Including Ground-Based Demonstration—The ground-based demonstration would consist of a one baseline system (three antennas) illuminated by three transmitters (two calibration transmitters and one beacon). Experiments which can be conducted include the following:

    a. Signal acquisition and phase measurements with pulsed transmissions (2 to 10 seconds).

    b. Space-angle measurement accuracy as a function of signal to noise.

    c. Phase measurement accuracy with simultaneous data transmission. This is desirable in order to keep transmission time minimum.

    d. Ambiguity resolution performance.

    e. Boom motion compensation using calibration signals (phases measured every 0.1 second).

    f. Multiple-access capability and adjacent signal rejection.

    g. Antenna misalignment effects.

3. Flight Experiment—This experiment would be conducted to demonstrate that booms can be deployed and can maintain the antennas pointed to the desired accuracy; to demonstrate that multipath effects can be kept to acceptable levels; to complete the demonstration of the concept; and to obtain data to allow an operational system to be designed and built.

Section 4

SIGNAL PROCESSING

4.1 EFFECT OF PHASE BIASES IN POSITION LOCATION VS. ATTITUDE SENSING INTERFEROMETER

In an interferometer system it is important to differentiate between phase biases and random errors. A phase bias is an error in phase produced by the interferometer or measurement circuits that is consistent for all phase measurements. This is in contrast to random phase errors due to thermal noise, for example. Phase biases may be time varying, but essentially constant with respect to the time for making phase measurements (calibration transmitters and beacons to be located).

In an interferometer used for attitude sensing, phase biases can be an important limitation in the accuracy of the system. Phase bias errors cannot be reduced by making repeated measurements, for example, as random errors can be.

In an interferometer used for position location, an entirely different situation exists. A phase bias which is the same for all measurements is two or three orders of magnitude less important than a random error of the same value. Thus it is important to differentiate between a "phase error" and a "phase bias." The reason for the above can be illustrated by use of Figure 4-1.

For an interferometer of baseline L, the phase measured across the baseline due to a transmitter R (ignoring random phase errors) would be

$$\phi_R = 2\pi\frac{L}{\lambda}\sin\epsilon + \phi_{bias} \qquad (4\text{-}1)$$

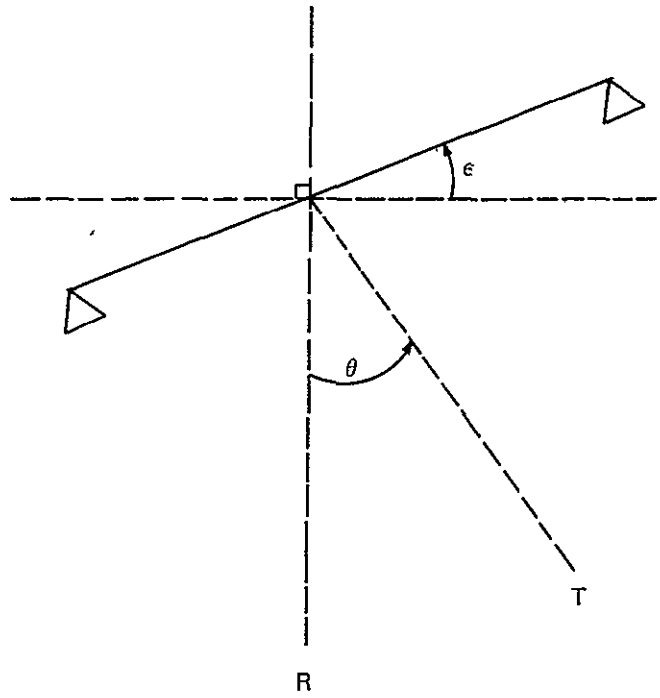

Figure 4-1. Interferometer Geometry

where

ϕ_R = measured phase for transmitter R
ϵ = angle of baseline with respect to wavefront from transmitter R
ϕ_{bias} = phase bias.

An unknown phase bias would obviously result in an error in the determination of the baseline angle ϵ.

The phase measurement due to a transmitter T would be

$$\phi_T = 2\pi \frac{L}{\lambda} \sin (E+\theta) + \phi_{bias} \tag{4-2}$$

For a position location application we wish to determine the angle θ between the transmitter at a known location R and the transmitter at an unknown location T. If we use the small angle approximation for the sines (angles will be less than 10^o) and solve for θ from the two equations, we find

$$\theta \cong (\phi_T - \phi_R) \frac{\lambda}{2\pi L} \tag{4-3}$$

Thus, position location determination is approximately independent of phase biases which are common to all calibration and beacon phase measurements.

In the proposed system, four calibration transmitters are used. With these it is possible to determine, on a continuous basis, the baseline length and orientation (two angles), and to obtain an estimate of the phase bias. This estimate further reduces the dependency of the system on phase biases. A detailed analysis of calibration was given in the Final Report (Phase I).

4.2 SIGNAL MULTIPLEXING AND PHASE RECOVERY

The diminished importance of phase biases for position location applications allows greater flexibility in signal multiplexing techniques which can be used in the satellite. Figure 4-2 illustrates two techniques. The only difference in the two techniques is the magnitude of the reference oscillator frequency f_r and the point where relatively narrow band filtering occurs. The incoming signals (calibration and beacon) will all be within a common frequency band of 30 kHz. In Case I, the signals from each antenna are kept separate by using a frequency f_r of 60 kHz and filtering signals from each antenna with 30 kHz filters before combining the signals. In Case II, a reference frequency of 2 kHz is used, and the signals are combined before filtering takes place.

The major advantage of Case I (separate spectrums) is that performance is better from a multiple access point of view, i.e., there is a smaller probability of overlap of signals from randomly transmitting balloons. The major advantage of Case II (combined antenna pairs) is that resultant phase biases are smaller. It was for this reason that this method was used for the ATS F&G breadboard interferometer which is an attitude sensor.

For the position location application the received signals (as indicated in Figure 4-2), after combining, would be upconverted and transmitted to the ground station. Figure 4-3 shows the signal processing required at the ground station, after the baseband signals are recovered, to recover the phase bearing signals from one antenna pair due to one transmitter.

A comb filter is used to locate the signals and set the voltage-controlled oscillator (VCO) to acquire the signal at frequency f_r. When the loop is in lock, the signal frequencies at the output of the mixer are at $f_o + f_r$, where f_o is the frequency of the loop offset oscillator. At this point, narrow-band filtering occurs (bandwidth of filters F_5 and F_6 typically 60 Hz and 200 Hz, respectively). The signal at frequency $f_o + f_r$ is translated to f_o by means of the recovered reference. The two signals at frequency f_o contain the desired phase information.

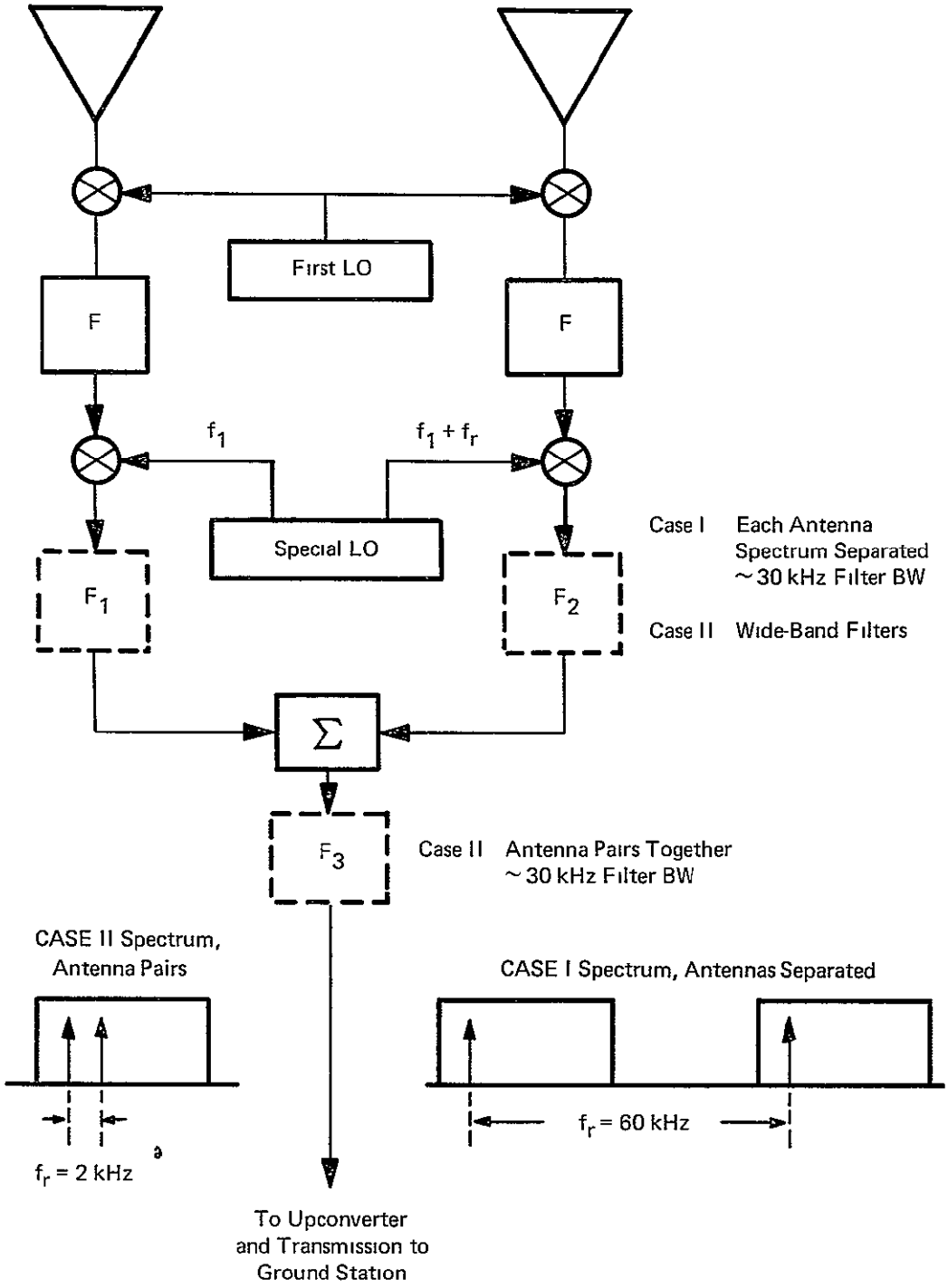

Figure 4-2. Two Signal Multiplexing Methods

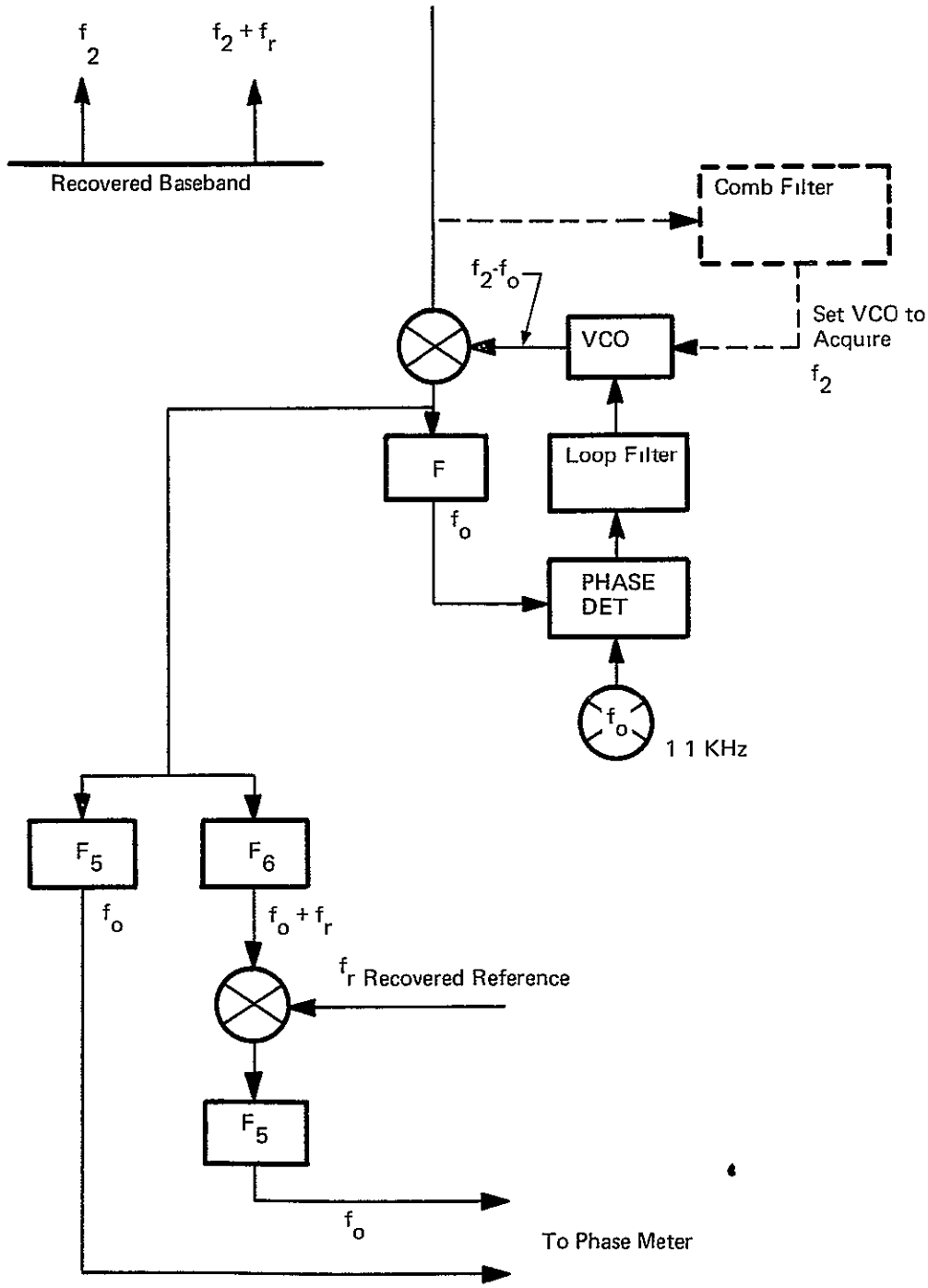

Figure 4-3. Signal Acquisition and Filtering, Ground Station

Table 4-1 lists possible sources of phase bias. Because the calibration and beacon signals are of different frequencies, entries in the Comments column indicate whether the phase bias is frequency dependent. The frequency sensitivity of the biases due to unequal cable lengths and antenna phase center are negligible (since $\Delta f/f = 10^{-5}$). The major frequency-dependent phase bias is a change in phase slope of a filter which contains only signals from one antenna, such as filters F_1 and F_2 in Figure 4-2. Note that the important item is phase tracking of two filters. The filters should be physically located together to maximize temperature, and therefore phase, tracking. These filters should also be designed for maximally flat time delay (or constant phase slope), such as afforded by the Gaussian filter.

It is possible also to make frequency-dependent corrections to measured phase. The frequency dependency of the phase can be determined, for example, by sweeping one of the calibration transmitters through the frequency range of the system. In the acquisition process, the signal frequencies are determined within 50 Hz in the comb filter. When the output of the phase-locked loop is used, the frequency can be determined more accurately.

Potentially the most damaging source of phase error is in the phase recovery circuit. The source of error would be in the narrow-band filters. Any change in phase of one filter with respect to the other will produce a random-like phase error in the measurement. The phase-locked loop will not contribute to the error. The loop need not be in complete phase lock because both signals which are to be compared in phase are equally affected.

It is possible, however, to calibrate the phase recovery circuits. For example, periodically the phase-locked loops can be locked onto the same signal, e.g., one of the calibration transmitters. Any residual error would now be a true phase bias. The important requirement of these phase recovery circuits is, therefore, that they be stable with time so that calibration will not be necessary too frequently. Calibration every hour would not be an excessive requirement.

Table 4-1

POSSIBLE PHASE BIAS SOURCES

Source	Comments
1. Unequal cable lengths in interferometer arms	Results in phase bias, slightly frequency sensitive (change of 0.001^{o} for 100^{o} phase bias and $\Delta f/f = 10^{-5}$).
2. Filters containing signals from one antenna	Such as F_1 and F_2 in Figure 4-5
a. Center frequency shift, one filter	Results in phase bias, frequency independent
b. Phase slope change, one filter	Results in phase bias, frequency dependent
3. Filters containing all antenna signals	Such as F_3 in Figure 4-5
a. Center frequency shift	No phase bias
b. Phase slope change	No phase bias
4. Error in phase of recovered reference f_r	Satellite reference oscillator, recovered on ground. Results in phase bias, frequency independent
5. Antenna phase center	Possibly small phase bias ($< 0.1^{o}$), function of angle of arrival of signal; slightly frequency-sensitive
6. Phase error in phase-locked loop recovery circuit	Due to lockup transient; no phase bias
7. Narrow-band filters in phase recovery circuit	Phase error (not phase bias) produced by unknown phase change in filter.

Section 5

GROUND PROCESSING EQUIPMENT DESIGN FOR FEASIBILITY TESTS

The ground processing equipment used in the feasibility tests includes a phase-locked loop, a phase recovery circuit, and a digital phase meter. The ground processing equipment requirements are discussed in subsection 5.1. The detailed design of the phase-locked loop, the phase recovery circuit, and the digital phase meter will be presented in subsections 5.2, 5.3, and 5.4, respectively.

5.1 GROUND PROCESSING EQUIPMENT REQUIREMENTS

The system requirements presented in Section 4 which affect the design of the ground processing equipment will be discussed in this section. These requirements will then be used to develop the design of the ground processing equipment. The configuration of the ground processing equipment may be used directly in the Case II multiplexing technique (see subsection 4.2) where a 2 kHz reference oscillator is used in the satellite. However, the results of the ground processing equipment experiments are applicable for both Case I and Case II multiplexing techniques. A discussion of the organization of the equipment, presented below, is useful before proceeding with the requirements.

It is convenient to segment the equipment into three functional items· the phase-locked loop, the phase recovery circuit, and the digital phase meter. A block diagram of the above items plus the interferometer is presented in Figure 5-1. The purpose of the phase-locked loop is to lock onto the proper signal pair within a certain spectrum (30 kHz for example) centered at 32.5 MHz which is an IF output of the ATS F & G breadboard interferometer. The signal pair is translated by the phase locked loop to the audio frequency spectrum

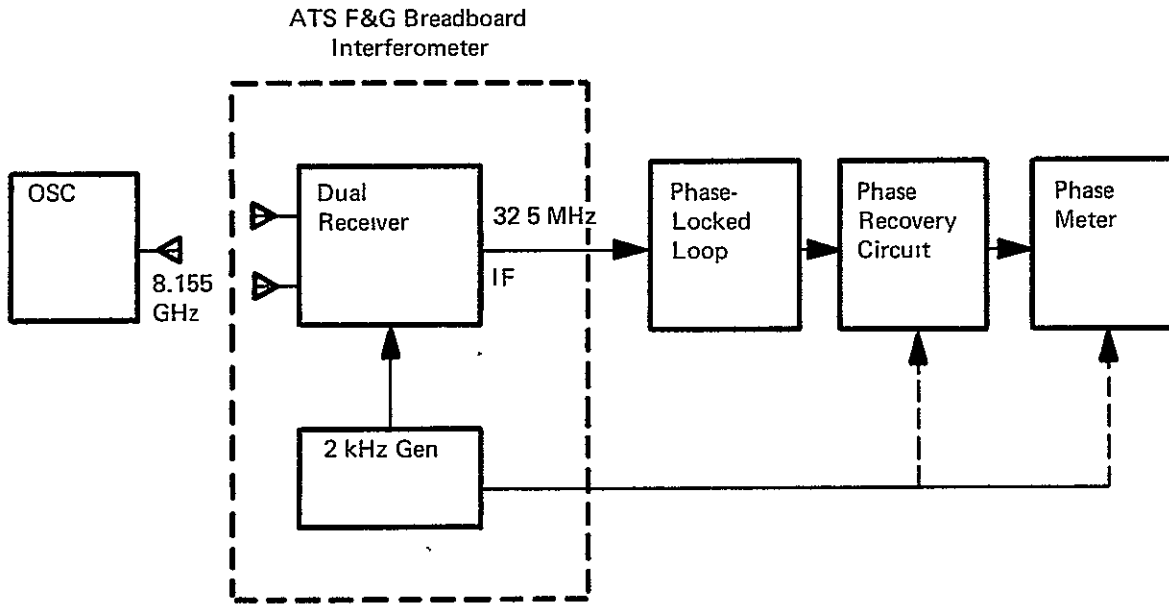

Figure 5-1. System Block Diagram for Experiment

where narrow-band filtering may be accomplished. The filtering takes place within the phase recovery circuit. The phase recovery circuit provides output signals from which the desired phase information may be extracted directly by the digital phase meter. The phase recovery circuit was designed initially so that the digital phase meter of the breadboard interferometer could be utilized. This resulted in one 2 kHz signal from the phase recovery circuit which served as an input to the phase meter (see Figure 5-2). The second input signal to the phase meter would be the 2 kHz reference signal.

The most critical portion of the equipment as far as phase stability is concerned is the phase recovery circuit. The configuration referred to above requires a bandpass filter in the phase recovery circuit having a center frequency of 3.1 kHz and a 3 dB bandwidth in the range of 20 to 60 Hz. The phase stability may be improved by decreasing the Q (center frequency divided by the 3 dB bandwidth) of the bandpass filters in the phase recovery circuit. An improved phase recovery circuit was designed midway through the program. This circuit resulted in narrowband filters centered a 1.1 kHz and 3 dB bandwidths of 60 Hz (see Figure 5-3). The resultant phase stability proved to be very satisfactory.

The improved phase recovery circuit used the 2 kHz reference signal to mix with one of the signal pair. The output of the circuit is two 1.1 kHz signals, and the phase difference between them is the desired phase information. The digital phase meter in the breadboard interferometer could not readily accomodate the two 1.1 kHz signals. Therefore, it was necessary to develop a digital phase meter.

5.2 PHASE-LOCKED LOOP DESIGN

The primary function of the phase-locked loop is to lock onto the signal pair and translate the signals to the audio frequency range where effective filtering may be accomplished in the phase recovery circuit. The loop was designed to meet the following requirements which are applicable to an operational system:

1. Rapid frequency lock.
2. A closed-loop bandwidth of approximately 50 Hz. This results in a minimum SNR of 10 dB which ensures that the loop will lock.

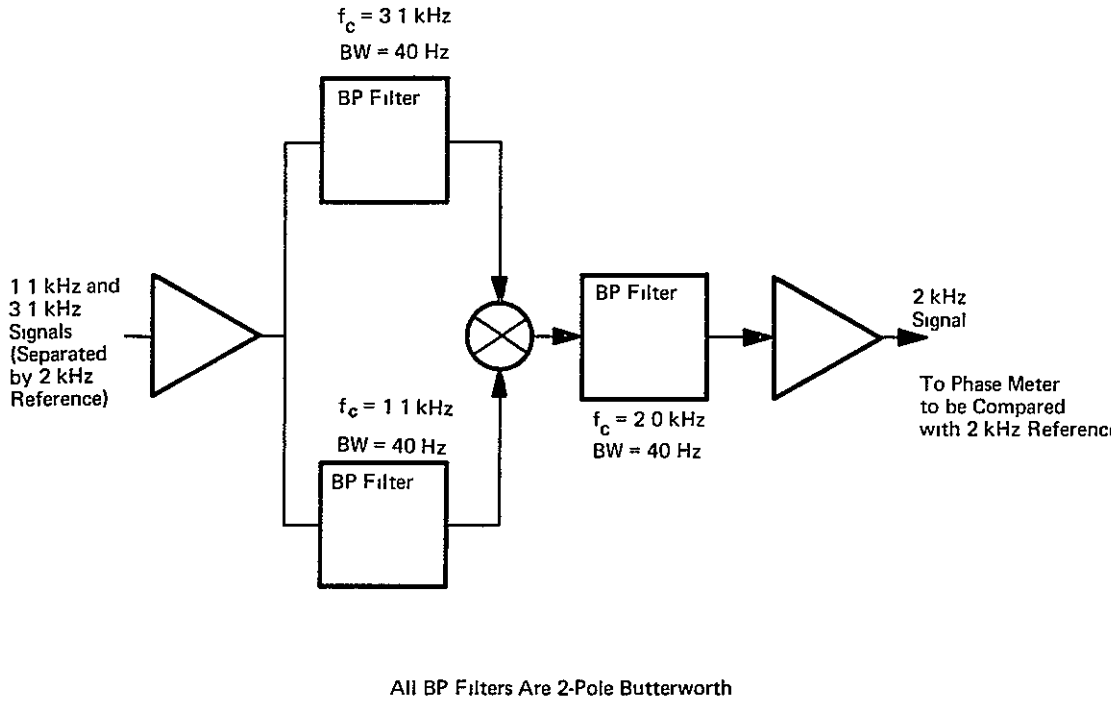

Figure 5-2. Block Diagram of Phase Recovery Circuit, Technique No. 1

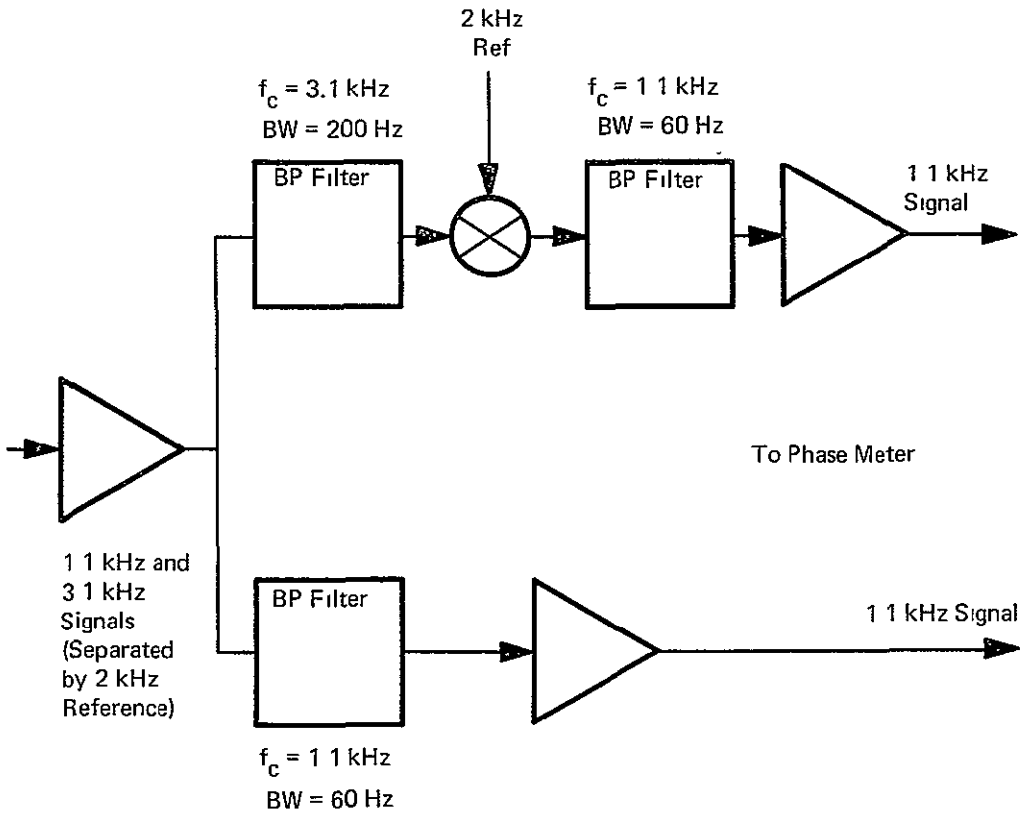

Figure 5-3. Block Diagram of Phase Recovery Circuit, Technique No. 2

In the experiment, the signals were CW with no bi-phase modulation. The loop, however, could be modified to meet the following requirement.

3. Capability of loop operation in the presence of 10 bps bi-phase data modulation.

A block diagram of the phase-locked loop is shown in Figure 5-4. The dotted blocks are the items which would have to be added to include the operation in the presence of 10-bit data modulation and an energy normalizing capability to increase the dynamic range performance of the loop. To translate the IF signals to 1.1 and 3.1 kHz, the output of the mixer is compared with an accurate 1.1 kHz reference signal (1×10^{-6} minimum frequency tolerance at room temperature). This particular frequency was chosen in order to minimize distortion effects in the mixer in the phase recovery. In an operational system, by means of comb filter acquisition circuits, the VCXO frequency would be set within 50 Hz of the frequency of the desired signal, so that lockup time will be of the order of milliseconds. The bandpass filter at 1.1 KHz prevents the loop from locking onto a stronger signal outside its passband. The bandwidth of the 1.1 KHz bandpass filter was sufficiently wide (200 Hz) to avoid affecting the stability of the loop adversely. The input level to the loop from the interferometer is -17 dBm for the signal pair or -20 dBm per signal. The breadboard interferometer has an AGC feature.

The requirements can be met adequately with a second-order loop. Although the second-order loop provides a phase-tracking capability, this is not of primary concern; it is the phase difference between the 1.1 and 3.1 kHz signals which is important, not the absolute phase. The expression for loop bandwidth for a second-order loop[6] is

$$B_L = \frac{AK + a}{4}$$

where

AK is the loop gain

a is the integrator gain of the loop filter.

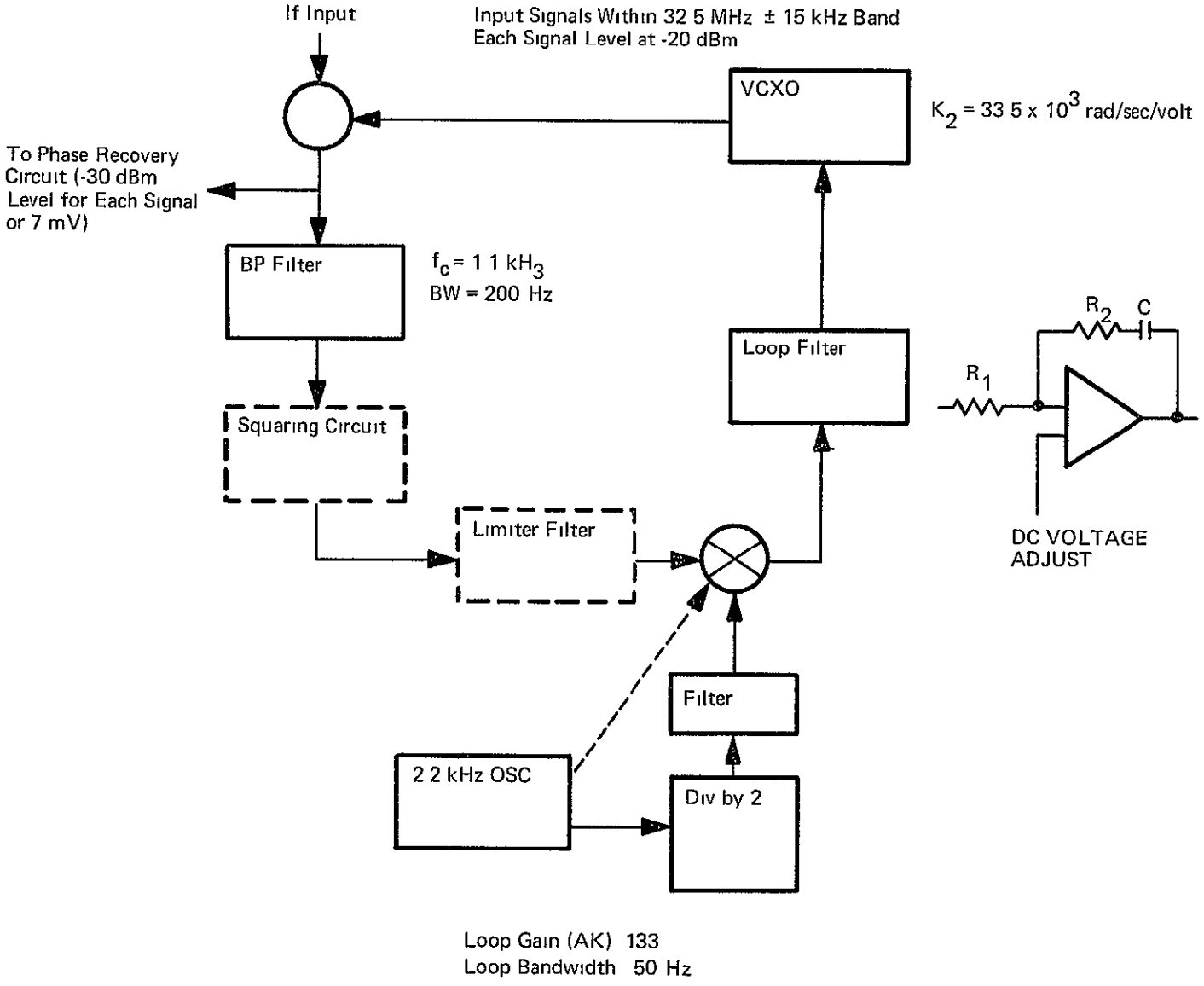

Figure 5-4. Block Diagram of Phase-Loched Loop

Reference 6 is used for the remaining portion of this development. The relationship between a and AK is determined by the damping factor of the loop. A damping factor of 0.707 is considered to be a reasonable compromise between stability and speed of response. This value for the damping factor results in

$$a = \frac{AK}{2}$$

and

$$B_L = \frac{1.5\ AK}{4}$$

The term AK must therefore be 133 to obtain a loop bandwidth of 50 Hz. The loop gain is determined as shown below.

$$AK = [A]\left[L_M\right]\left[G_{BPF}\right]\left[L_P\right]\left[L_{PD}\right]\left[G_{LF}\right]\left[K_2\right]$$

where

A	is the input signal level in volts
L_M	is the mixer loss
G_{BPF}	is the gain of the bandpass filter. The filter is active, thereby having the potential of gain.
L_P	is the loss of a pad between the bandpass filter and phase detector
L_{PD}	is the loss of the phase detector
G_{LF}	is the high frequency gain of the loop filter
K_2	is the VCXO constant in radians/second/volt.

The apportioning of these terms to obtain the desired AK is straightforward and is not discussed in detail. The bandpass filter is a one-pole active filter. The details of this type of filter are discussed in subsection 5.3. The VCXO will swing $\pm$ 16 kHz at a center frequency of 32.5 MHz for a $\pm$ 3V input signal resulting in $K_2 = 33.5 \times 10^3$ rad/sec/volt. The high-frequency gain of the loop filter is R_2/R_1, (the ratio of the feedback resistor to the input resistor).

The transfer function of the filter is

$$F(s) = \left[1 + \frac{a}{s}\right] G_{LF}$$

$$= \left[1 + \frac{1}{R_2 CS}\right] \frac{R_2}{R_1}$$

where

$$\frac{1}{R_2 C} = \frac{AK}{2}$$

The purpose of the voltage adjustment of the operational amplifier is to set the VCXO frequency near the desired input signal.

The loop could be designed to operate in the presence of bi-phase data modulation and have an energy normalizing capability by incorporating the dotted blocks in Figure 5-4. The squaring circuit would remove the bi-phase modulation and would create a CW signal at 2.2 kHz. This would be filtered to remove the harmonics and limited. The output from the limiter would be filtered and compared with a 2.2 kHz reference signal in the phase detector. This filtering is not too critical since the only function is to remove harmonic frequencies.

5.3 PHASE RECOVERY CIRCUIT DESIGN

The design of the phase recovery circuit will be discussed in this section. The two techniques for the phase recovery circuit will be presented first. A comparison will be made between the two techniques followed by a discussion of the design of the technique chosen for development. The section will be concluded by a description of the active filters which were used to realize the filters.

5.3.1 Phase Recovery Circuit Techniques

In this subsection, discussion of the two phase recovery circuit techniques will be presented and the techniques compared on the basis of requirements.

The primary requirement of the phase recovery circuit is to filter each signal of the signal pair and to provide output signals from which the phase information can be extracted. A high degree of phase stability with respect to time and, to some extent, temperature must be maintained. The quantitative requirements are given below:

1. The peak-to-peak phase measurement should be within 0.6 degree over a 1-hour period. This is approximately equivalent to 0.1 degree, 1 sigma, which is the portion of the total instrumentation error budget (0.3 degree, 1 sigma) which was allocated to the phase recovery circuit. This stability should be accomplished over the expected variation of room temperature. The integration time is not critical since it is the slow drifts due to temperature variations that are of primary interest.

2. The filters should be designed to minimize the effects of CW interfering signals on the phase measurements while at the same time meeting the peak-to-peak phase measurement requirement.

3. The phase recovery circuit should meet requirement 1 over an input signal strength range of 10 dB. This simplifies design of AGC circuits which can extend the dynamic range.

There is a tradeoff between requirements 1 and 2 which will be discussed before the two techniques are compared. Any discrimination requirement may be met by the use of filters of a sufficiently narrow bandwidths (while still passing the signal energy) and complexity (number of poles and filter design type such as Butterworth). However, the phase slope in the passband generally increases as the filter discrimination is increased, and the phase stability will degrade as shown below. Therefore, the filtering must be a compromise between the two requirements. The phase sensitivity of a filter with respect to temperature is given below:

$$K_T = T_s \phi_s f_c$$

where

K_T is the phase sensitivity of the filter in electrical degrees per degree C

T_s is the ratio of the filter center frequency change to the filter center frequency per degree C

ϕ_s is the phase slope of the filter at the center frequency (degrees per Hz)

f_c is the center frequency of the filter (Hz).

The phase sensitivity K_T, therefore, may be decreased by reducing any of the three variables. For example, filtering should take place at as low a center frequency as possible.

The block diagram of the first technique is shown in Figure 5-2. The 1.1 kHz and 3.1 kHz signals are mixed together after filtering, and the difference signal passes through the 2.0 kHz bandpass filter. The phase of this signal is compared with the phase of the 2 kHz reference signal to obtain the desired phase information. The filter designs were selected to obtain a high degree of discrimination while at the same time attempting to meet the 0.6-degree peak-to-peak phase stability. This technique requires narrow-band filtering before the mixer in order to minimize the mixer losses when two noisy signals are mixed together.

It was difficult to obtain even a small dynamic range with this configuration because both inputs to the mixer were, of course, changing. It was believed that the problem was due to the mixer impedances varying with signal strength thereby introducing undesired phase shift. Normalizing one or both of the signals can alleviate this problem. If at least one of the signals can be maintained at a high level (greater than +3 dBm), the mixer should maintain a fairly constant impedance. This was not necessary since this was not a serious problem with the second technique.

The block diagram of the second technique is shown in Figure 5-3. Since the 3.1 kHz signal is mixed with the relatively noise-free 2.0 kHz signal, narrow-band filtering at 3.1 kHz is not required. The difference signal is filtered in a 1.1 kHz bandpass filter. A similar bandpass filter is used in the 1.1 kHz channel. The desired phase information is obtained by measuring the phase difference between the two 1.1 kHz signals. Since the two narrow-band filters are of the same design, drift in the two filters will cancel to a large degree when the phase comparison is made. The 2.0 kHz input to the mixer can be maintained at a

high and fairly constant level, thereby ensuring a more constant mixer impedance with varying signal strength as compared with the first technique. It was concluded that the second technique would be used in the final breadboard.

5.3.2 Design of the Phase Recovery Circuit

5.3.2.1 Filter Design

The filters were designed to obtain the maximum degree of discrimination while at the same time satisfying the phase stability requirement. There is a design tradeoff between the filter bandwidth, number of poles, type of design (that is, Butterworth, Chebishev, Bessel, etc.) and the phase response which results from the three preceeding parameters. It would be advantageous if the filter had as few poles as possible in order to minimize the cost of the phase recovery circuit. Therefore, it was decided to achieve the filtering by narrow bandwidths and few poles per filter as opposed to wider bandwidths and more poles per filter. In addition, this would result in more discrimination near the center frequency because of the narrower bandwidth as well as a higher signal-to-noise ratio as input to the phase meter.

The two 1.1 kHz filters were used to determine the discrimination. A reasonable compromise for these filter parameters appeared to be a 2-pole Butterworth design filter with a 60 Hz bandwidth. A 1-pole filter did not give sufficient discrimination for a bandwidth which would give acceptable phase stability performance. The 3.1 kHz filter was chosen to be a 2-pole Butterworth filter with a 240 Hz bandwidth. This filter provides adequate filtering at the 900 Hz image frequency. Also, it affords some protection against overloading the mixer with interfering signals.

The phase stability of the phase recovery circuit may be determined from Figure 5-5, which is a plot of the expression for K_T for a 2-pole Butterworth filter and T_s = 100 ppm/^{o}C. In the next subsection this value of T_s will be shown to be reasonable for the filters. K_T is given by

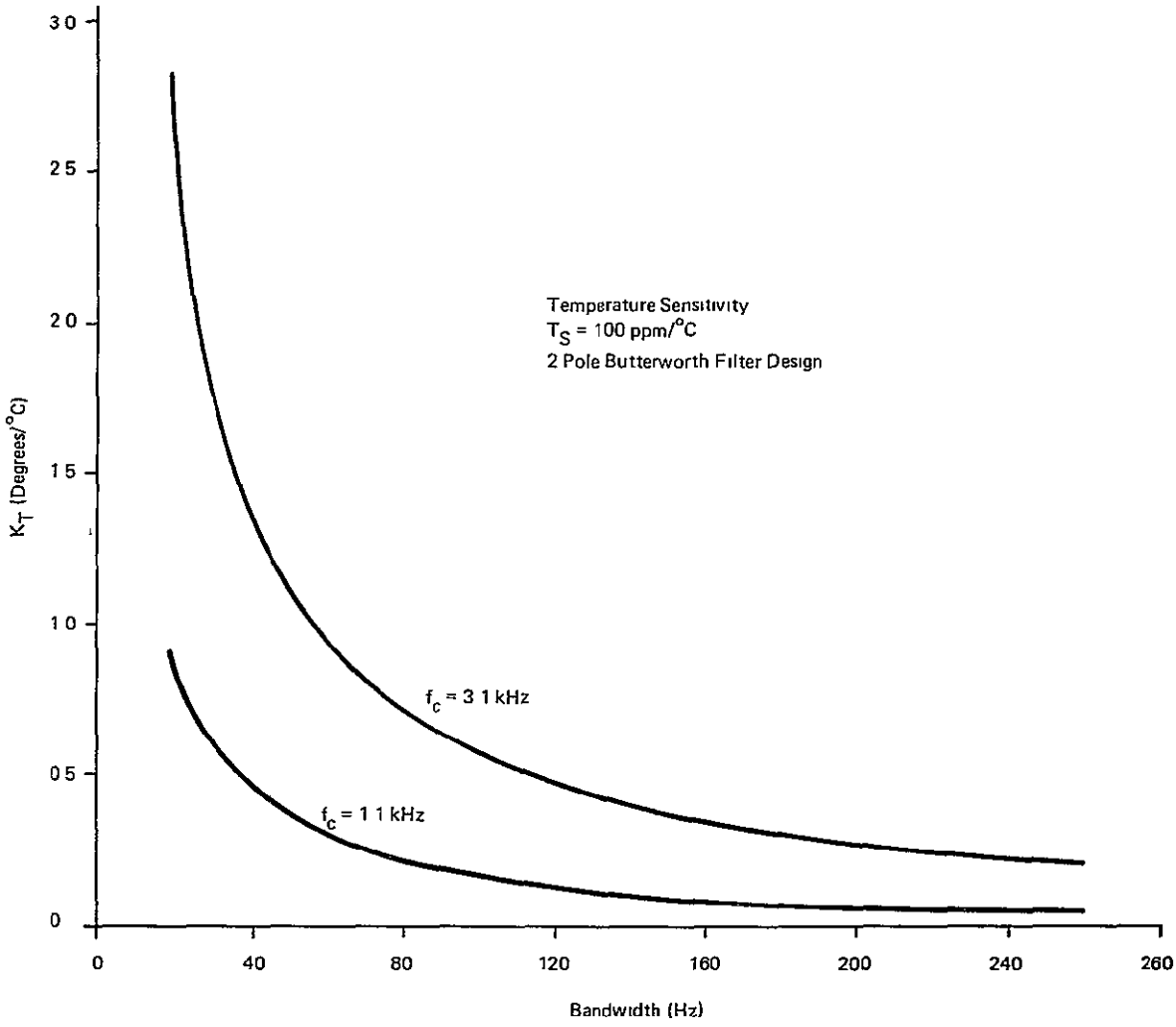

Figure 5-5. Phase Sensitivity to Temperature vs. Bandwidth

$$K_T = K_T \text{ (3.1 kHz filter)} + K_T \text{ (1.1 kHz filter)} - K_T \text{ (1.1 kHz filter)}$$
$$= [\,0.22 + 0.34 - 0.34\,] \text{ degree}/^{\circ}C$$
$$= 0.22 \text{ degree}/^{\circ}C$$

Even if the phase stabilities of the 1.1 kHz filters cancelled only to within 20%, the circuit phase stability would be determined primarily by the 3.1 kHz filter. Narrowing the bandwidth of the 1.1 kHz filter in the 1.1 kHz channel would further compensate for the above phase stability. This was not attempted during this development. It was felt that a $1^{\circ}C$ variation in temperature over 1 hour would be reasonable. The remaining portion of the 0.6° peak-to-peak phase stability requirement was reserved for the effects due to the 10 dB variation in signal strength.

5.3.2.2 Phase Recovery Circuit Implementation

It was first necessary to select an approach for the filter implementation. The following requirements were desired of the filter:

1. High Q over the lower audio frequency range
2. Low sensitivity with respect to temperature
3. Ease of varying the bandwidth and center frequency.

The latter requirement was due to the experimental nature of the program. The RC active network appeared to be the most appealing solution for the filter implementation.

Interest in the use of active networks has been increasing over the past several years. An article by Sallen and Key in 1955 discussed 18 RC amplifier resonators.[7] Many of these and subsequent circuits were found to be useful for applications requiring low values of Q. Recently, active circuits have been developed which are characterized by high values of Q and low sensitivity to element deviations caused by temperature and aging. One such circuit receiving attention is described in references 8, 9, and 10. The stages are connected as a controlled positive feedback loop. Any one of the three following transfer functions may be obtained from the same circuit by taking the output from the proper output port.

$$T(s) = \frac{a}{s^2+ms+p} \quad \text{(lowpass)}$$

$$T(s) = \frac{s^2 b}{s^2+ms+p} \quad \text{(highpass)}$$

$$T(s) = \frac{sc}{s^2+ms+p} \quad \text{(bandpass)}$$

Each network may be used to realize two poles for a lowpass and highpass design or one pole for a bandpass design. For example, a 5-pole bandpass filter may be realized by the use of five active networks previously described. Each network would realize one of the poles. The sensitivity and Q of the network are determined essentially by the RC components used in the integrators. Circuits having Q values of several hundred in the audio frequency range and thermal coefficients (f_c in parts per million per degree C for the bandpass circuit) of a few parts per million per degree C at room temperature are presently in use.[8, 9]

Several single-pole (for bandpass configuration) active filters were purchased from Kinetic Technology, Incorporated. A detailed theoretical and practical discussion of the filters is found in reference 10. The circuit configuration is as shown in Figure 5-6. The pertinent specifications of the filter are listed below:

Typical Q at 1000 Hz	500
Typical Q at 20 kHz	250
Typical Q at 50 kHz	75
f_c stability (-30°C to +85°C)	100 ppm/°C typical
	300 ppm/°C maximum
Power Consumption	250 mW
Typical d.c. voltages	$\pm$ 15V
Dimensions (excluding leads)	0.8 x 0.5 x 0.4 in.

The small physical size is possible because of the hybrid integrated design of the circuit. The filter may be mounted in a 14-pin dual in-line

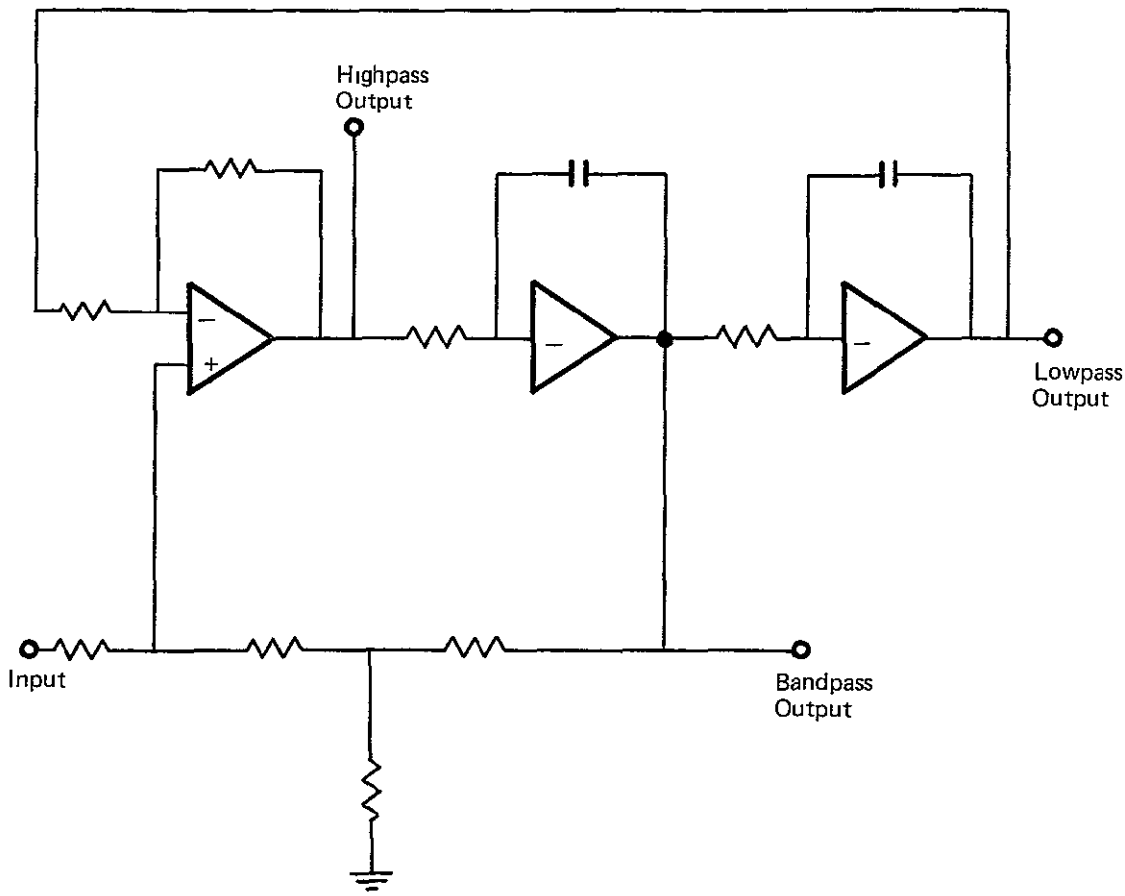

Figure 5-6. Diagram of an Active Filter

1C receptacle. The wide range of temperature for this f_c stability is to be noted. It is believed that lower values of f_c stability may be obtained if the circuit is operated at room temperature. This is supported by data presented in reference 9.

External components are used with the network to obtain the desired center frequency and bandwidth. A number of adjustment techniques are available. The one used for this program requires the use of two approximately equal valued resistors to adjust the center frequency and one resistor to adjust the bandwidth. The two adjustments are approximately independent.

The schematic for the phase recovery circuit is shown in Figure 5-7. The maximum signal level at the input of the phase recovery circuit for one signal of the signal pair is approximately 7 mv. This will provide a +3 dBm level signal at the R port of the mixer input which is the maximum level required to achieve the useful 10 dB dynamic range. This will be shown in subsection 5-4. The gain of 50 was apportioned between the input operational amplifier (gain of 10) and the first filter in each channel (gain of 5). The mixer loss is approximately 8 dB. The gain of the 1.1 kHz filter in the 3.1 kHz channel is 5. The gain of the two output operational amplifiers are such as to produce output voltages of 3.2 volts rms for the input conditions stated above.

The external resistors used with the filters are 1% metal-film resistors having a maximum temperature coefficient of 100 ppm/^{o}C. It is likely that the resistors determine the temperature coefficient of the filters when operating near room temperature.

5.4 DIGITAL PHASE METER

The purpose of the digital phase meter is to convert the phase difference between the two 1.1 kHz signals into a digital count. This is accomplished by shaping both sine waves into square waves, enabling a gate with the leading edge of one square wave, and disabling it with the leading edge of the other. While the gate is enabled it passes a 4.5056 MHz square wave to a counter. Thus, the

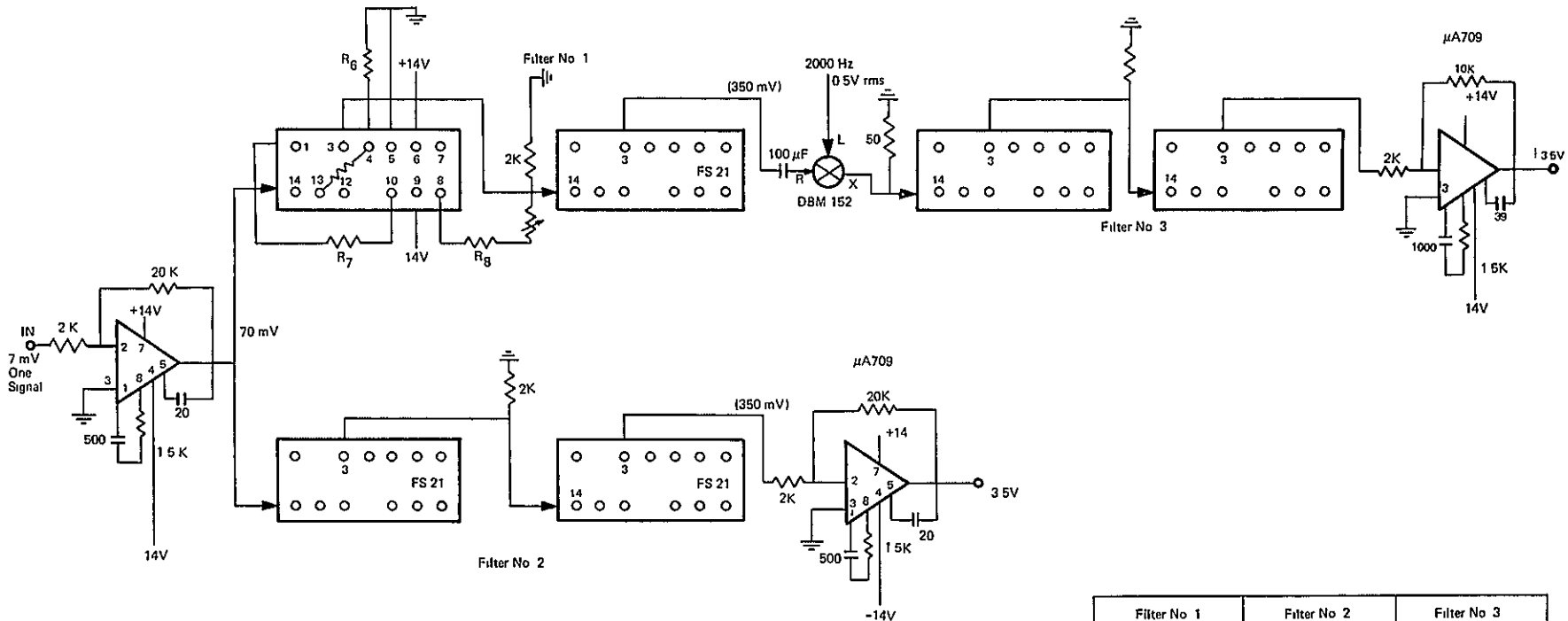

	C_F (Hz)	BW (Hz)
Filter No 1	3100	250
Filter No 2	1100	60
Filter No 3	1100	60

	Filter No 1		Filter No 2		Filter No 3	
	Stage 1	Stage 2	Stage 1	Stage 2	Stage 1	Stage 2
Center Freq (Hz)	3 009	3,192	1 079	1,121 4	1,079	1,121 4
Bandwidth (Hz)	162	170	41 5	43 5	41 5	43 5
Voltage Gain	3 2	3 2	3 2	3 2	3 2	3 2
R_7 (Ohms)	16 600	15,900	46 645	44 880	46 645	44,880
R_8 (Ohms)	16 600	15,900	46 645	44 880	46,645	44,880
R_6 (Ohms) **						
R_0 *						

* After tuning for center freq , adjust R_0 for proper gain

**Then, adjust R_6 for proper bandwidth

Check CF gain and BW

Figure 5-7. Phase Recovery Circuit, Technique No. 2

maximum single-sample count observable is 4096. Resolution of the meter is therefore 0.09°. A block diagram of the converter breadboarded for the present effort is shown in Figure 5-8. It contains logic which enables the gate every 16th cycle of the 1.1 kHz signal and terminates sampling after 64 samples have been taken. The maximum count observable after this operation, which takes approximately 1 second, is 4096 x 64 = 262,144.

Figure 5-9 is a logic diagram of the meter. The zero crossing detectors (ZCDs) square the sinewave. The 270° delay prior to the $\div 16$ logic is necessary to enable the gate at the proper time to pass every 16th cycle to the remainder of the converter. The count-64 chain is preceded by a 1.5τ delay so the 64th pulse can be fully processed before the operation is stopped. The leading edges of the two square waves are differentiated and used to set and reset a flip-flop. The flip-flop, set by the first wave, enables a gate which allows the second wave to pass. The output of the second differentiator is inhibited during the output of the first differentiator to prevent premature reset of the flip-flop when the phase difference is greater than 180°. Ambiguity zone detection/correction circuitry was not included in this early model, so the output will be unreliable in the vicinity of 0°, depending upon signal-to-noise ratio.

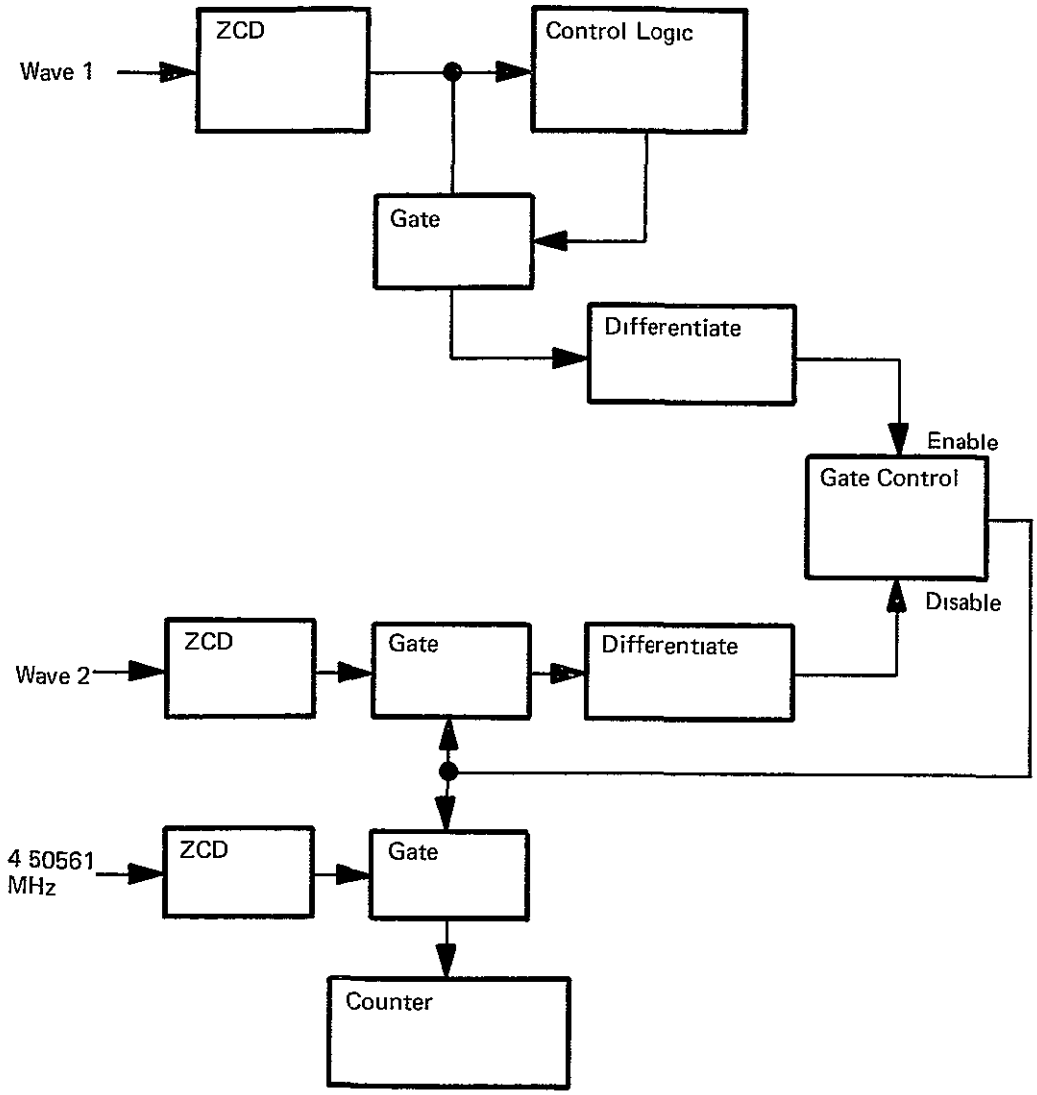

Figure 5-8. Digital Phase Meter Block Diagram

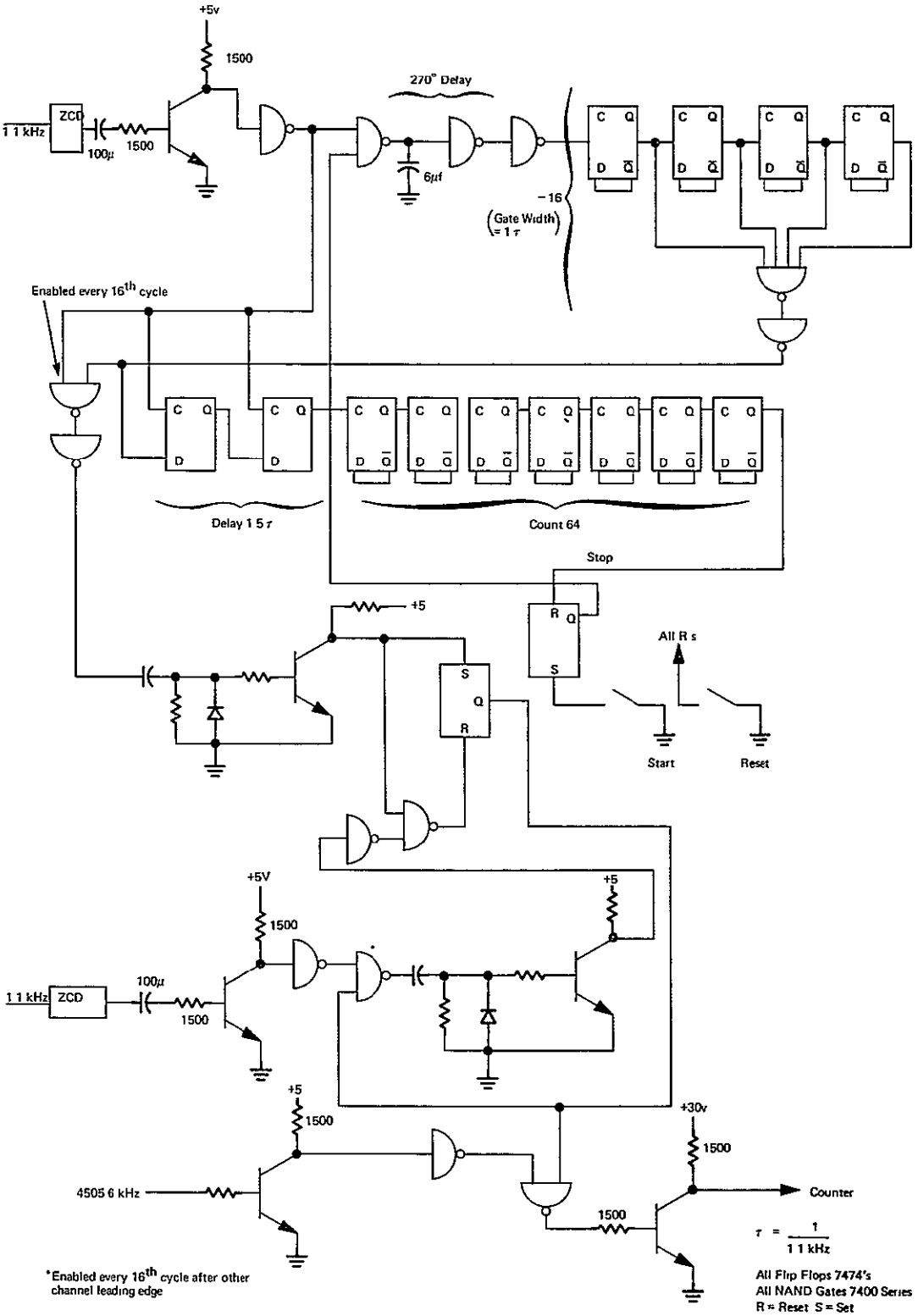

Figure 5-9. Digital Phase Meter, Logic Diagram

Section 6

TEXT RESULTS OF PHASE RECOVERY CIRCUIT

The phase recovery circuit is the most difficult part of the ground processing equipment to implement and potentially the most critical with respect to phase stability, dynamic range, and interference. Therefore, the phase recovery circuit was tested extensively. The amplitude and phase response of various active filters were measured first, including those in the phase recovery circuit. In all cases, the measured responses were almost identical to the theoretical responses. A test signal generator which would generate 1.1 and 3.1 kHz signals from accurate 1.1 kHz and 2.0 kHz oscillators was designed and assembled. This was used for most of the tests of the phase recovery circuit.

The phase stability of the phase recovery circuit was measured with respect to time at room temperature using the test signal generator. The Wiltron phase meter was used for all phase stability measurements. The lowest bandwidth of 10 Hz was used, resulting in an integration time of approximately 100 ms. This integration time was sufficient, since the purpose of the tests was to measure the long-term drift in phase due to normal room temperature variations. The same test was performed using the interferometer and injecting a signal at 8.155 GHz. The phase shift as a function of temperature was then measured from 40°C to 24°C (105°F to 75°F). The phase shift vs. signal level was measured to determine the available dynamic range. The phase recovery circuit was also tested for discrimination against interference signals.

6.1 TEST SIGNAL GENERATOR

A method was needed to create stable 1.1 and 3.1 kHz signals. The block diagram of the test signal generator which performs this function is

shown in Figure 6-1. The 1.1 kHz and 2.0 kHz are signals which are stable to at least 1×10^{-6} at room temperature, which is sufficient as will be shown later. The 1.1 kHz signal serves either as an input to the first mixer when bi-phase data modulation is desired or as an input to second mixer when no modulation is desired. The 3.1 kHz signal is obtained by mixing the 1.1 kHz signal with the 2.0 kHz signal. A 900 Hz signal is also present but is filtered adequately in the phase recovery circuit. The 2.0 kHz signal is also used as the reference signal input to the phase recovery circuit. The bandpass filters were single pole and realized with the same active networks described previously.

6.2 AMPLITUDE AND PHASE MEASUREMENTS

The loss and phase responses of the 1.1 kHz filter in the 1.1 kHz channel of the phase recovery circuit are shown in Figure 6-2. The results compare favorably with the theoretical curves. The loss response of the 3.1 kHz channel which includes the two filters is shown in Figure 6-3. The response of the 1.1 kHz channel is also shown in this figure so test the responses of the two channels may be compared. The differential phase shift between the two channels is shown in Figure 6-4, and the slope is seen to be approximately 0.7 degree per Hz. This compares favorably with the computed slope of the 3.1 kHz bandpass filter. This data was obtained by varying the 1.1 kHz signal in the test signal generator. The phase slope of the 3.1 kHz filter may be obtained by varying the 2.0 kHz signal in the test signal generator. The same slope resulted, thus verifying that the differential phase slope in the phase recovery circuit is almost entirely due to the 3.1 kHz filter. It is also concluded from the above data that only very modest frequency stabilities are required of the 1.1 kHz and 2.0 kHz oscillators. That is, a 10^{-5} frequency stability for the 2.0 kHz oscillator would result in a phase error of 0.014 degree.

6.3 PHASE STABILITY AT ROOM TEMPERATURE

The phase stability of the phase recovery circuit at room temperature was measured using the test signal generator, the Wiltron phase meter, and an XY recorder as shown in Figure 6-5. The integration time of the phase meter was

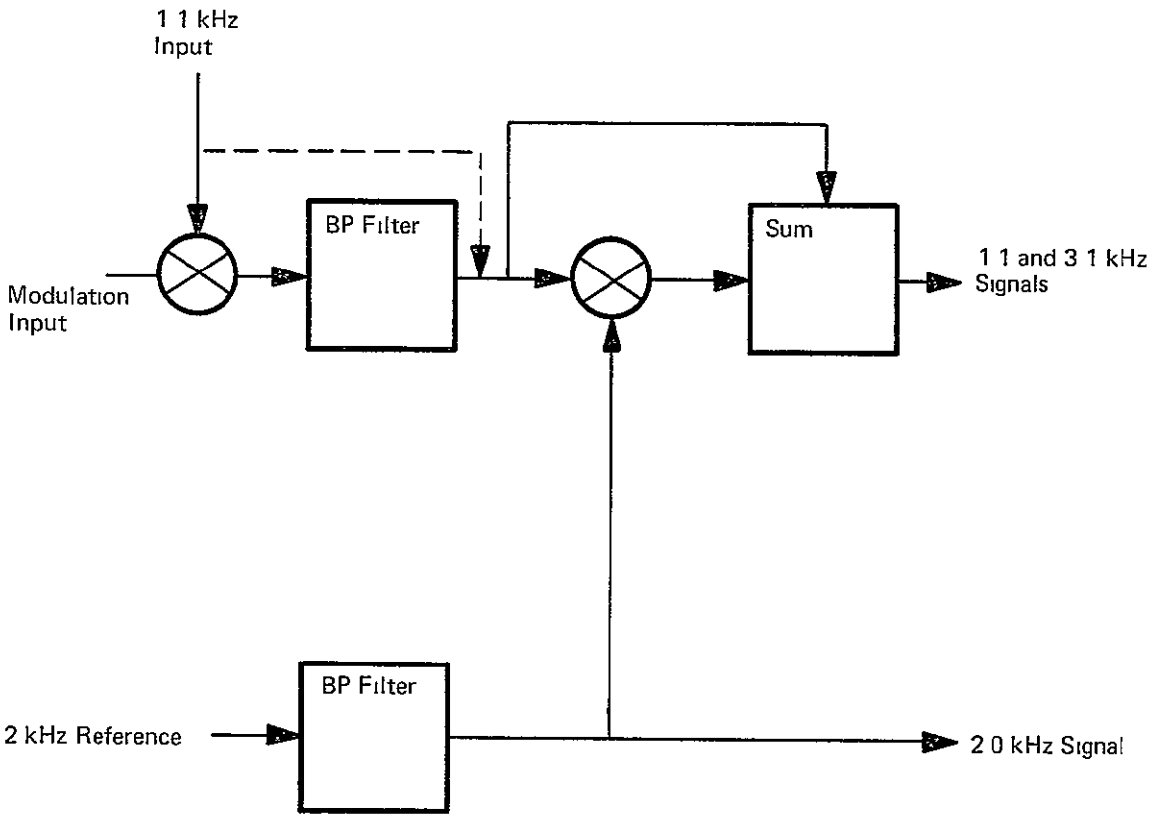

Figure 6-1. Block Diagram of Test Signal Generator

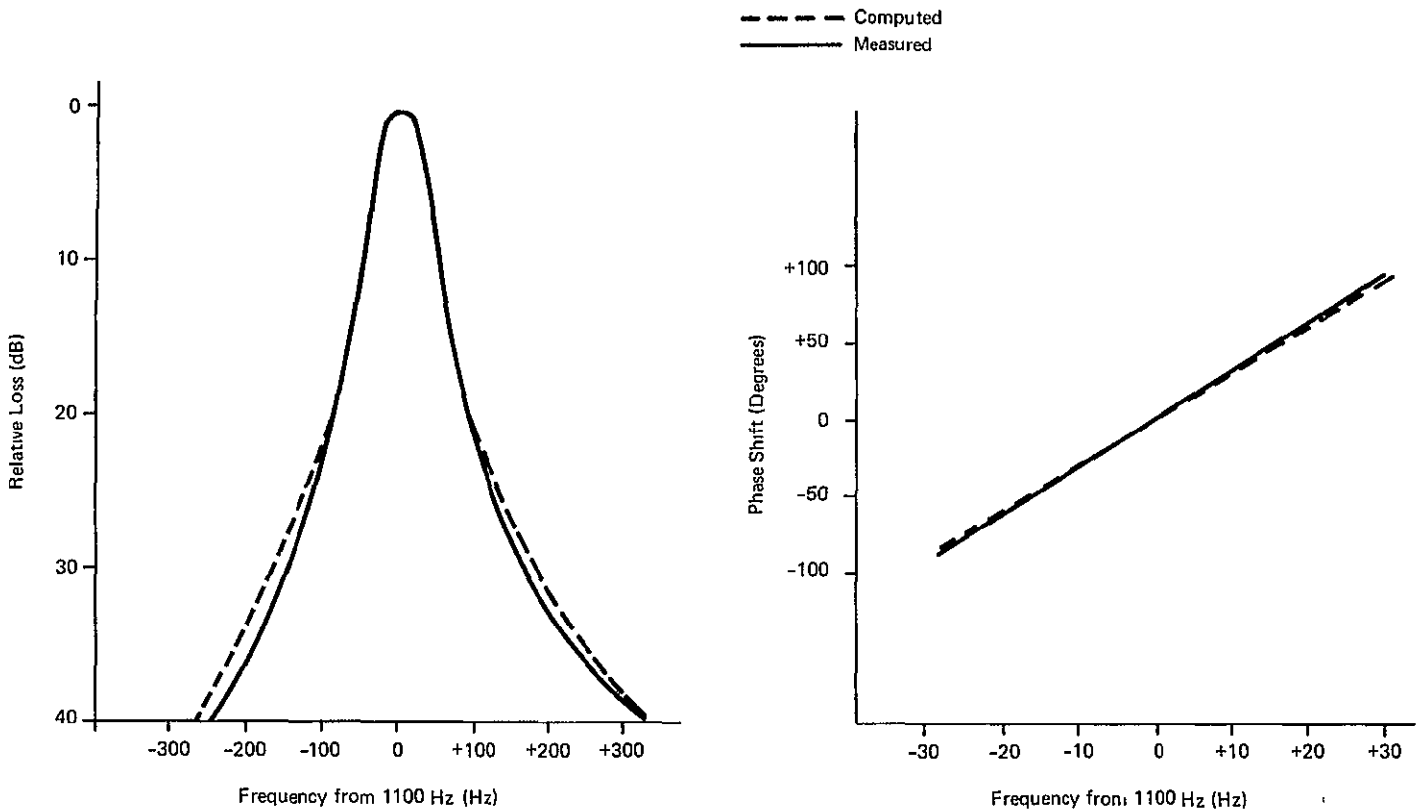

Figure 6-2. Measured Response of 1100 Hz Filter

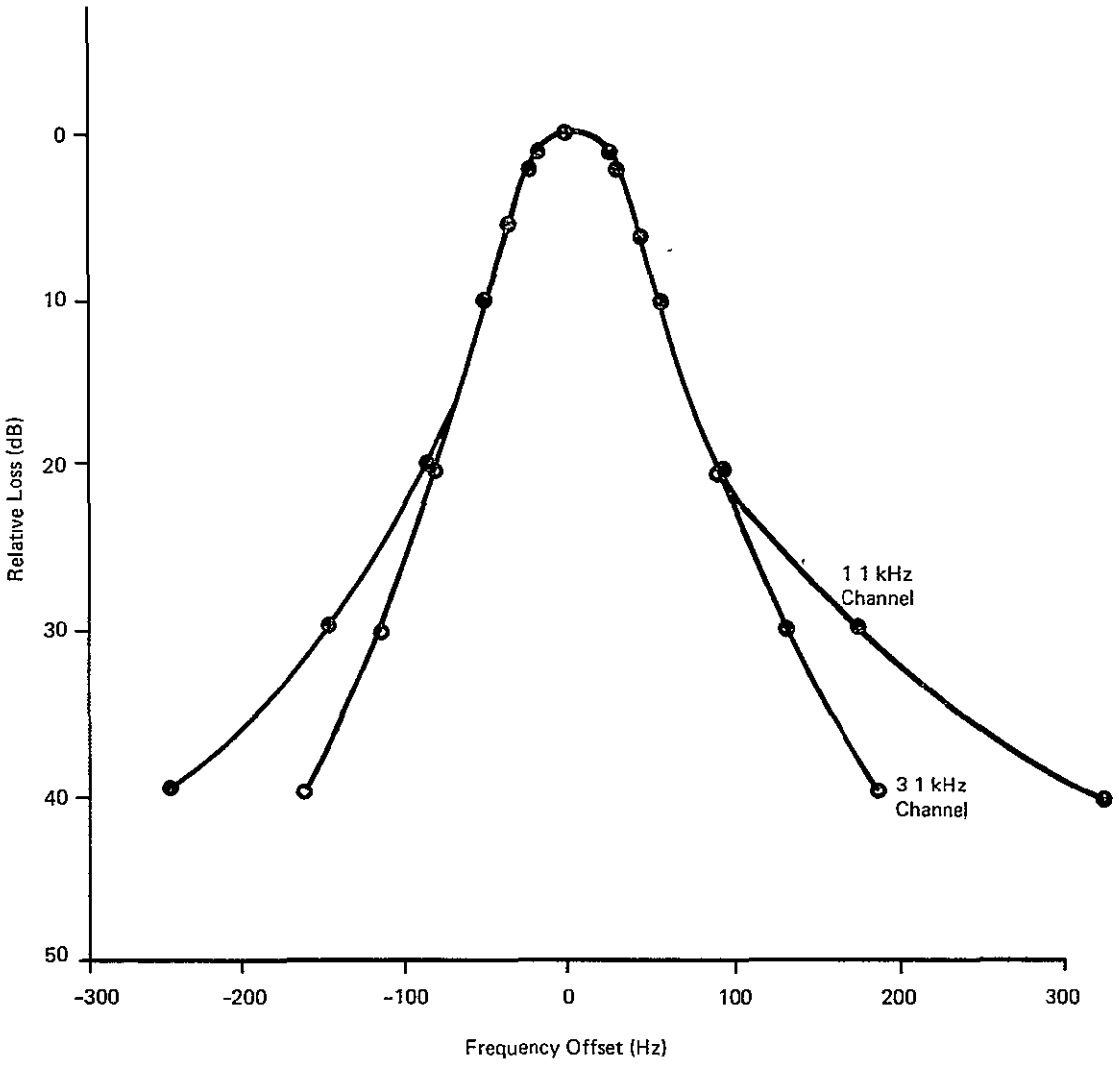

Figure 6-3. Filter Loss vs. Frequency

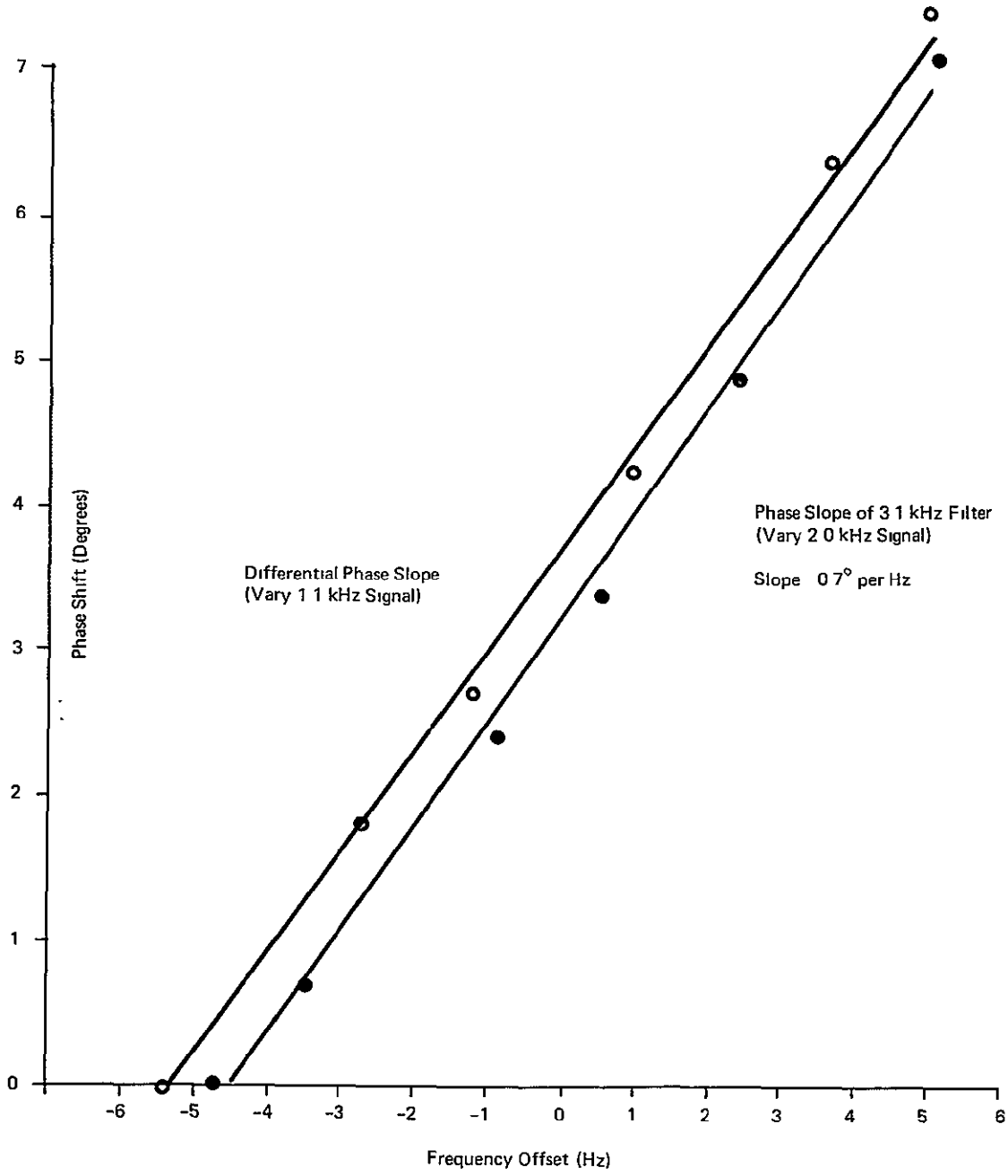

Figure 6-4. Phase Shift vs. Frequency Offset

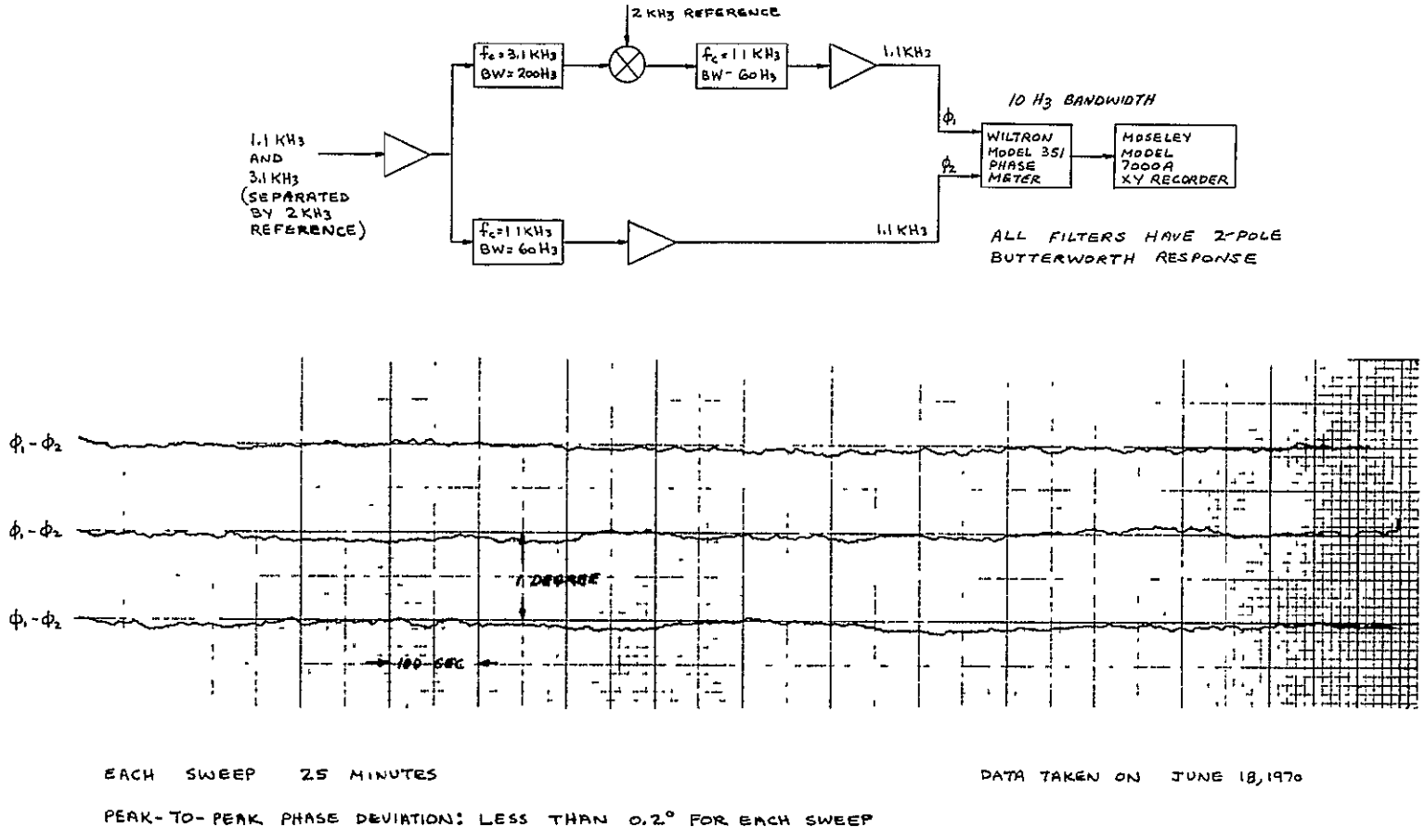

Figure 6-5. Phase Stability of Phase Recovery Circuit

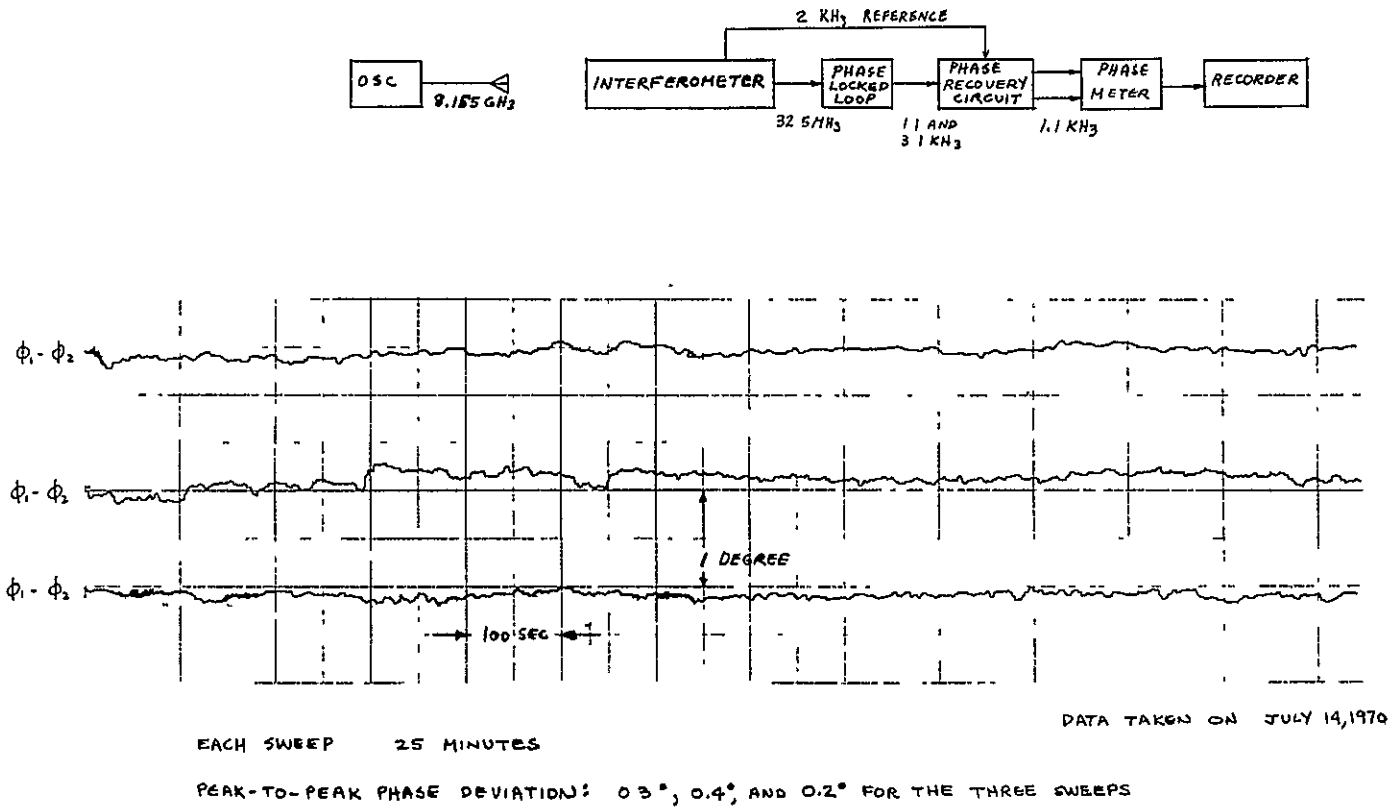

Figure 6-6. Phase Stability with Interferometer

100 ms. This corresponds to the minimum averaging time for the phase measurements in the system concept design. The peak-to-peak phase variation was less than 0.2 degree per 25-minute sweep. It is recalled that the calculated phase variation per ^{o}C was 0.22 degree. It seems reasonable to expect a temperature variation of about 1^{o}C. The same data was taken using the interferometer and injecting a signal at 8.155 GHz. The measured phase variation per sweep was 0.2 to 0.4 degrees peak-to-peak with a maximum variation over the 75 minute period of 0.4 degrees. (See Figure 6-6.)

6.4 PHASE SHIFT VS. TEMPERATURE

The phase recovery circuit was placed in a temperature chamber, and the temperature was varied from 40^{o}C to 24^{o}C and then from 24^{o}C to 40^{o}C. The input signals were obtained from the test signal generator. The data is plotted in Figure 6-7. The resulting phase slope of 0.2 degree/^{o}C compares very closely to the predicted slope of 0.22 degree/^{o}C.

6.5 DYNAMIC RANGE

The main limitation of the dynamic range appeared to be due to the mixer in the phase recovery circuit. The most useful signal range was for the R port signal power to vary from -4 to -14 dB with respect to the L port signal power (constant at approximately +7 dBm). The results are plotted in Figure 6-8. A 10 dB dynamic range resulted in a 0.2-degree phase error. Once again the input signals to the phase recovery circuit were obtained from the test signal generator, and the levels of both signals were varied simultaneously. No attempt was made to thoroughly analyze the effects of the mixer on dynamic range. It is believed, however, that it is the nonlinear effect of the mixer which results in the dynamic range limitation. The results discussed above represent a significant improvement over those for the other phase recovery circuit technique, which required that both signals into the mixer be varied with signal strength variation. The 0.2-degree error over a 10 dB dynamic range was considered to be adequate. The dynamic range can be readily extended with an AGC circuit.

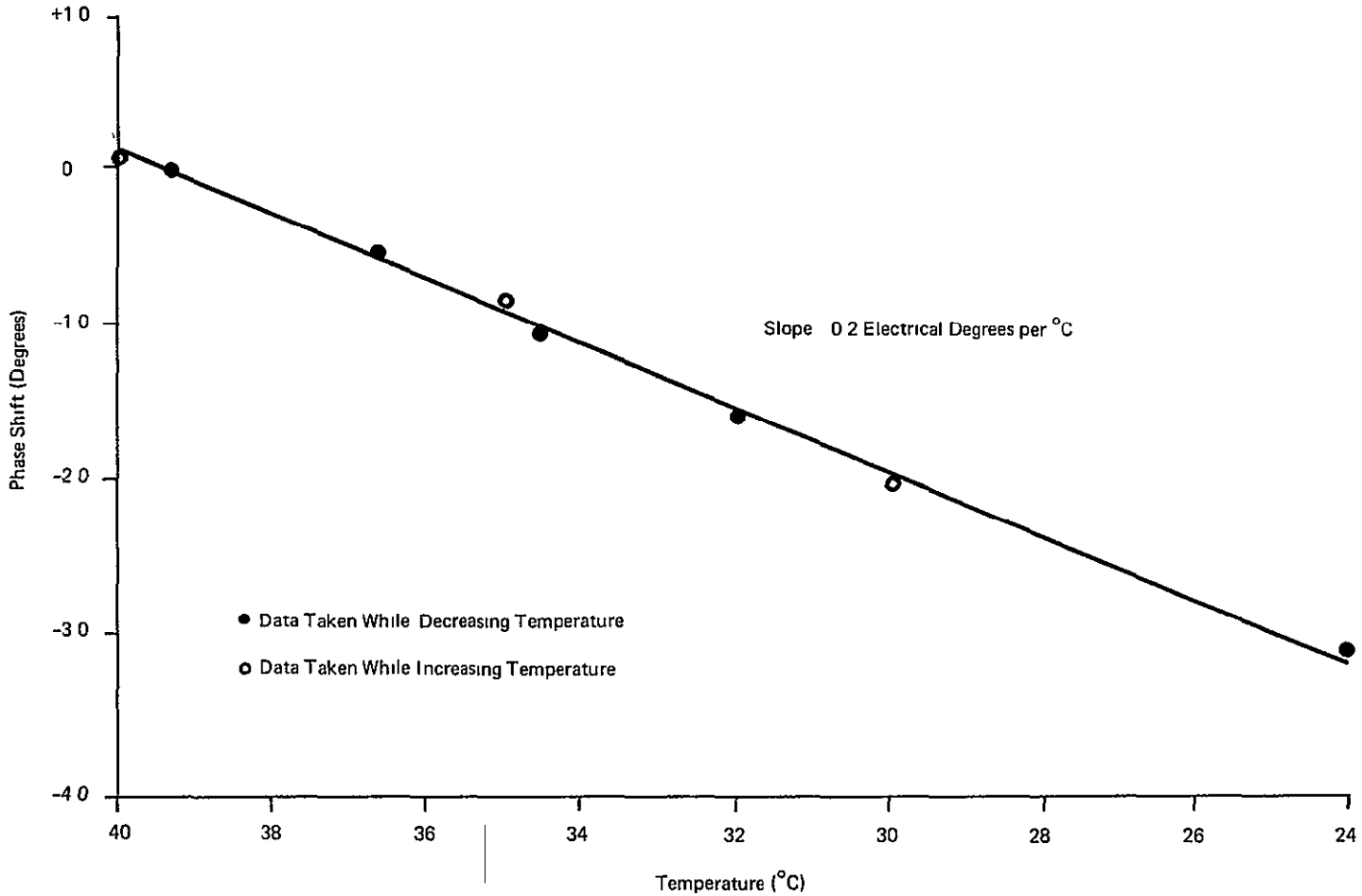

Figure 6-7. Phase Shift vs. Temperature

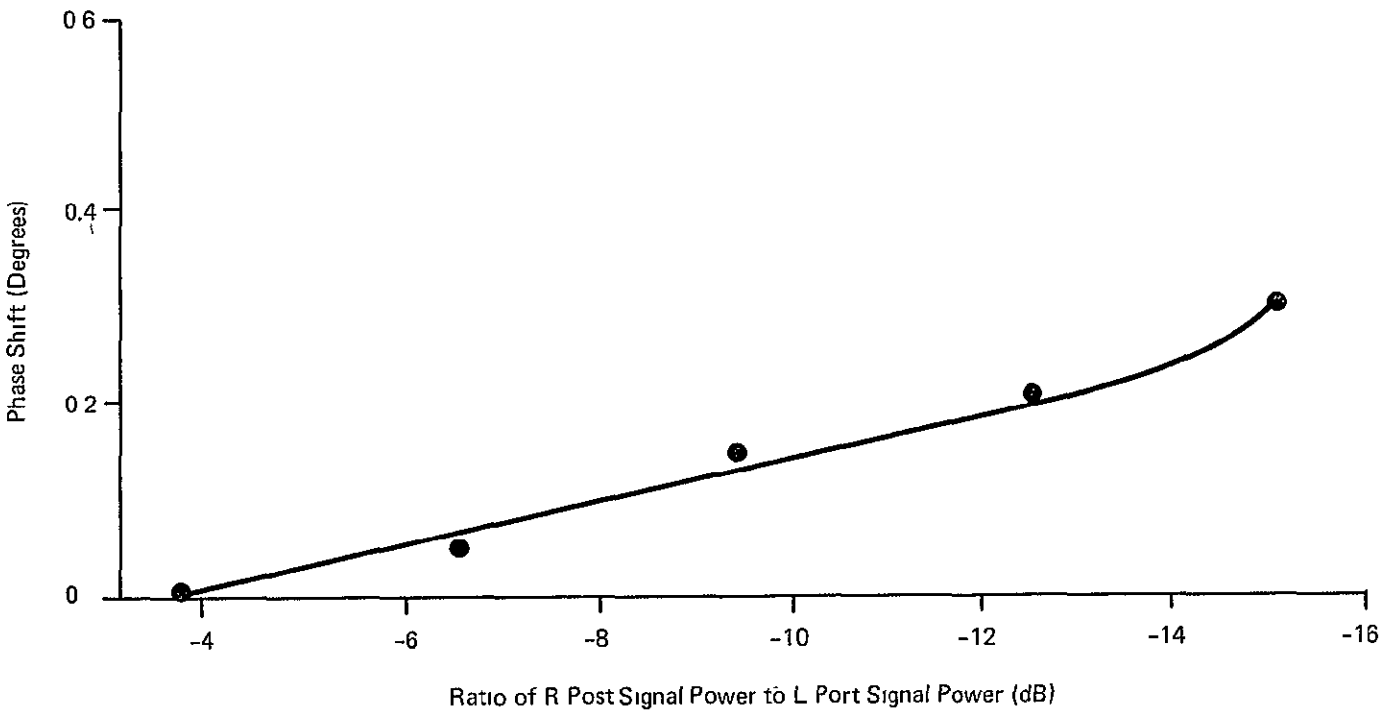

Figure 6-8. Phase Shift vs. Signal Level

6.6 INTERFERENCE TESTS

The interference tests were performed by injecting a CW signal of various levels and frequencies into the summation network of the test signal generator and measuring the resulting phase error. The phase shift was measured by the Wiltron phase meter. The results are shown in Figure 6-9. Consider the case of an interfering signal 20 dB higher than the desired signal. If it were injected near (in frequency) the 1.1 KHz signal, the frequency of the interference signal must be approximately 95 Hz removed from 1.1 kHz to obtain a 1.0-degree phase error and removed by approximately 115 Hz to obtain a 0.3-degree phase error. The 3.1 kHz channel is more sensitive to interfering signal levels because of the presence of the mixer. The attenuation of the 3.1 kHz bandpass filter is not sufficient to prevent the interfering signal to overdrive the mixer. It is seen that an offset of approximately 25 Hz would result in a negligible phase error for an interfering signal whose level was equal to that of the desired signal.

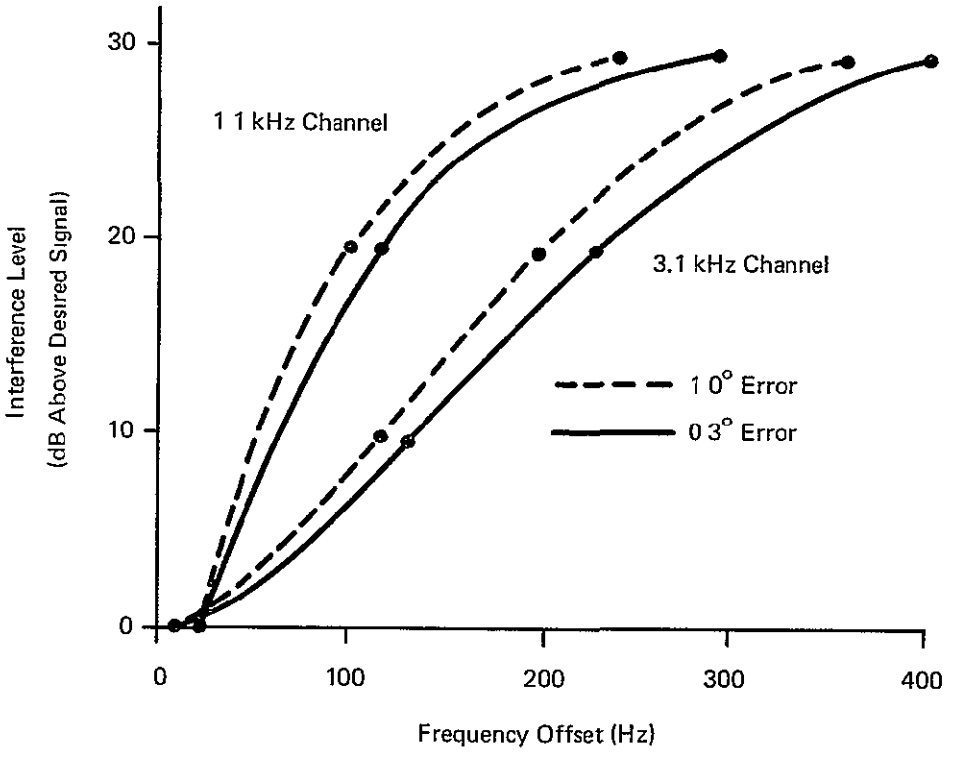

Figure 6-9. Interference Level for Given Phase Error

Section 7

CALIBRATION TESTS

7.1 PURPOSE OF EXPERIMENTS

Several calibration experiments were conducted utilizing the breadboard ATS-F interferometer. These experiments were designed to show that:

1. The relative angle between two illuminators could be measured to $+0.003^{\circ}$ (1σ) for a 26.6λ system. Then for a 400λ baseline with all else remaining the same (e.g., same antenna phase center stability and phase errors), the relative angle accuracy could be extrapolated to $\pm 0.0002^{\circ}$ (1σ). This corresponds to a position location error of $\overline{0}.2$ km from synchronous altitudes.
2. The accuracy of the relative angle is independent of the orientation of the baseline. The object here is to substantiate the choice of the satellite attitude control specifications which does not require precise (e.g., less than 1 degree) attitude sensing and control.
3. The length and orientation of the baselines can be calibrated to requisite accuracies by measuring the phases from two illuminators at known separation angles. This is a test of the stability of the antenna phase centers, i.e., ideally, the estimated baseline length should be independent of the illumination angle.
4. The accuracy of the relative angle between illuminators is much less sensitive to phase bias errors then to phase errors caused by, for example, thermal noise. The significance of this test is to show that rather large phase biases that could be introduced by the satellite and ground terminal circuits do not grossly degrade the position accuracy.

7.2 EXPERIMENT DESCRIPTION

The breadboard ATS-F interferometer was mounted in an anechoic chamber which had been modified to accommodate two (rather than a single) illuminators. No special tests were made to determine how much this affected the chamber performance (reflection or multipath signals).

Furthermore, the relative sizes of the interferometer and the chamber required certain adjustments to the math models used to transform phase information into angle information. These adjustments to the math model led to the introduction of additional parameters for which only estimates could be made. All such parameters affect the accuracy of the results to some extent.

Figure 7-1 is a schematic of the experiment and lists the parameters required by the math model with their estimated values. Values d_t and d_r were estimated by taping the distance from the interferometer center of rotation to each illuminating antenna. Possible sources of error were:

1. The exact center of rotation was unknown because of the manner of mounting the interferometer on the totating pedestal
2. The taped distance was from the surface of the illuminating antenna which does not account for the fact that the phase center was inside the antenna
3. The center of rotation could be a function of ϵ (orientation).

An analysis was made to determine the effect on the experiment due to errors in d_t and d_r. The analysis indicated that probable errors in the parameters ($\pm$1 inch) would not significantly degrade the experimental results. Post-experiment data processing analyses also verified this conslusion (see Figure 7-5).

Value θ was estimated by a different technique. The interferometer was turned on, allowed to stabilize, and then rotated until the phase across the coarse and vernier baselines from the reference antenna indicated zero. The TRAV-A-DIAL reading was then set to zero. Next the target antenna was turned on, the reference antenna turned off, and the interferometer rotated until the phase across the vernier baseline again read zero. Value θ was read directly off the TRAV-A-DIAL. This test was conducted several times. A best estimate of θ was established as $5.66^{\circ} \pm 0.0025^{\circ}$. The TRAV-A-DIAL has a resolution of $\pm 0.0025^{\circ}$.

The estimate of L_v was taken from the ATS-F interferometer final reports based on a precision mechanical measurement of the distances between the

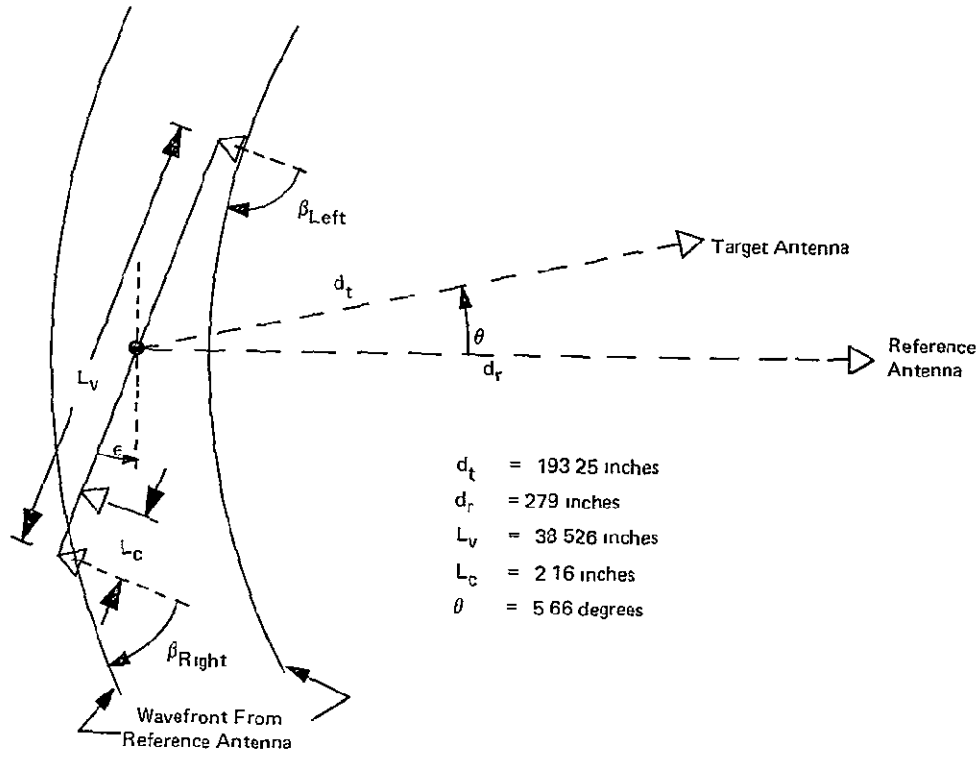

Figure 7-1. Interferometer Array Illumination Geometry in Anechoic Chamber

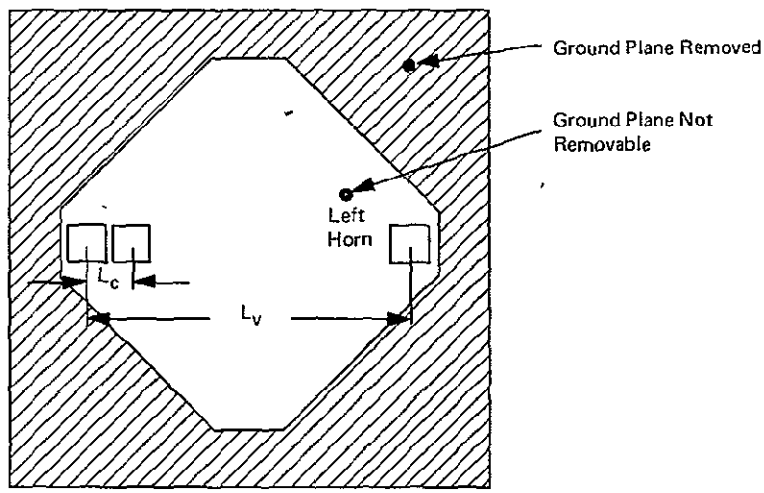

Figure 7-2. Interferometer Array Layout Showing Removable Ground Plane Portion

geometrical centers of the antennae. L_c, the coarse baseline length, was obtained likewise.

The best estimate of the phase bias was taken as zero. Great care was used in the ATS-F interferometer design and fabrication to remove all biases.

The math model assumed that all antennae (interferometer plus illuminators) were within 0.1 degree of being in a common plane for all orientations. An analysis indicated that the assumption was not critical.

With a satellite-borne interferometer, d_t and d_r are so large that the math model becomes independent of these parameters. In particular, considerations such as the exact center of rotation and the possible translation of this center with baseline orientation can be neglected. Also, in the chamber, the interferometer antennas do not have the same illumination angle (see β_{right} and β_{left}, Figure 7-1) because the wavefronts are spherical. Thus the phase center stability problem is aggravated more in the chamber than in a satellite application. Some of these problems were investigated briefly and are discussed in a subsequent section.

7.3 EXPERIMENT RESULTS

Three sets of data were taken. The first set (referred to hereafter as the basic data set) was taken with the interferometer unchanged from its ATS-F status. The second set of data was taken with the L. H. antenna rotated 180°. Due to the mechanical design, this rotation could be made precisely with only a minute possibility of mechanical translation. The third set of data removed a portion of the large ground plane surrounding the interferometer antennae (see Figure 7-2).

All three sets of data were then processed in a variety of ways; the two more significant being to test the consistencies of the relative angle, θ, versus baseline orientation, ϵ, and the length of the baseline, L_v, versus orientation.

Figure 7-3 gives the results for all three data sets and shows the near independence of the relative angle, θ, with baseline orientation. The data trends were derived from a least squares fit to a quadratic; that is, the data was assumed to be in the form:

$$\Delta\theta = \Delta\theta_o + \theta'\epsilon + \theta''\epsilon^2 + \text{Noise}$$

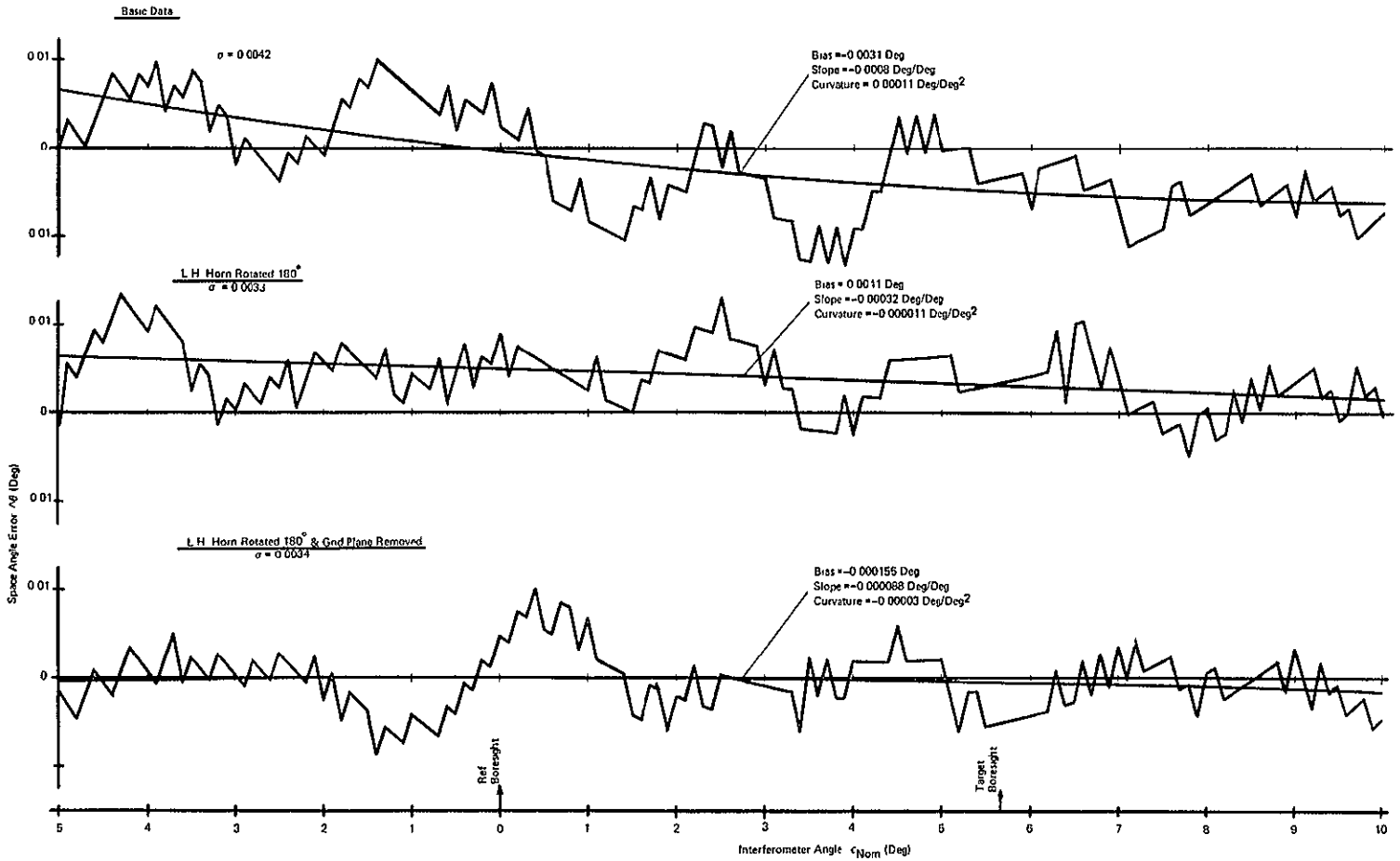

Figure 7-3. Data Trends vs Modifications to Interferometer Antennae Orientation and Ground Plane

where

$\Delta\theta$ = Θ-5.66°

$\Delta\theta_o$ = Bias

θ' = Slope

θ'' = Curvature

ϵ = Orientation (see Figure 7-1)

If the relative angle θ were truly independent of ϵ, then $\Delta\theta_o$, θ' and θ'' would all be zero. It will be shown that a likely cause of $\Delta\theta_o$ is an error in the estimate of L_v, $\hat{\Delta L}_v$, whereas a likely cause of θ' is a phase bias. Several factors contribute to θ''.

The square root of the sum of the residuals is called σ where a residual is the difference between the computed value and the data trend at that value of ϵ. If, by suitable adjustment to the parameters, all data trends were removed, some degree of irregularity would remain. These irregularities are a measure of the randomness of the data caused by quantization error in the digital phase meter and upredictable changes to the parameters caused by a change in orientation. Since the desired accuracy was 0.003 degree, the σ indicates that this has been achieved. The data was recorded in tenth degree increments of ϵ as measured by the TRAV-A-DIAL. The most rapidly varying part of the residuals can be attributed to the quantization error in the digital phase meter. If a curve were drawn through the residuals so as to smooth through these quantization errors, there would remain a relatively slowly varying residual for which no clearcut explanation can be made at this time. Note that this slowly varying curve does not correlate well in phase among the three data sets, though the peak amplitudes are quite similar.

One explanation proposed as the source of the slow variations was multipath. The chamber was modified to accommodate the target illuminator which negated to some unknown extent its anechoic properties. However, if multipath were

simply a consequence of adding the target illuminator, then rotating the L. H. antenna could not reasonably be expected to alter the multipath signals; therefore the basic data set and L. H. horn rotated by 180° set should correlate well. However, this does not seem to be the case. Consider especially the $-2 < \epsilon < 2$ region. Removing a portion of the ground plane could certainly have affected the multipath; and as the bottom curve shows, there is little correlation with either of the other two.

Another possibility for the slowly varying residuals is a shift in the antenna phase centers due to a complex interaction between the interferometer horns and the ground plane. Field distortions produced by this ground plane could warp the antenna characteristics; and since these field distortions would depend on the angle of incidence, among other things, the warpage would depend on the orientation. In this case, rotating the horn 180° would not necessarily correlate with any other data set because the interaction would change. Likewise, removing a portion of the ground plane would infer that there should be little correlation because this too would change the interaction.

The ground plane originally simulated the front face of the ATS-F EVM (Earth Viewing Module). Its mechanical design and fabrication was such that the entire ground plane could not readily be removed. Therefore, no further experiments were conducted.

In summary, there is no discerning evidence that points to a particular source of the slowly varying residuals. It is our opinion that the ground plane-antenna interaction is the most likely source, however.

Figure 7-4 shows the results of processing the three data sets under a different set of assumptions. In Figure 7-3, L was assumed known and θ was solved for. Here, θ is presumed known and L is solved for. As would be expected, the correlation of the respective data sets subject to two different assumptions is almost perfect; that is, the top curves in figures 7-3 and 7-5 should, except for the ordinates, appear similar. However, the magnitude of the ΔL variations is important since for a satellite application these unpredictable variations (those not completely compensated for by the calibration) must be

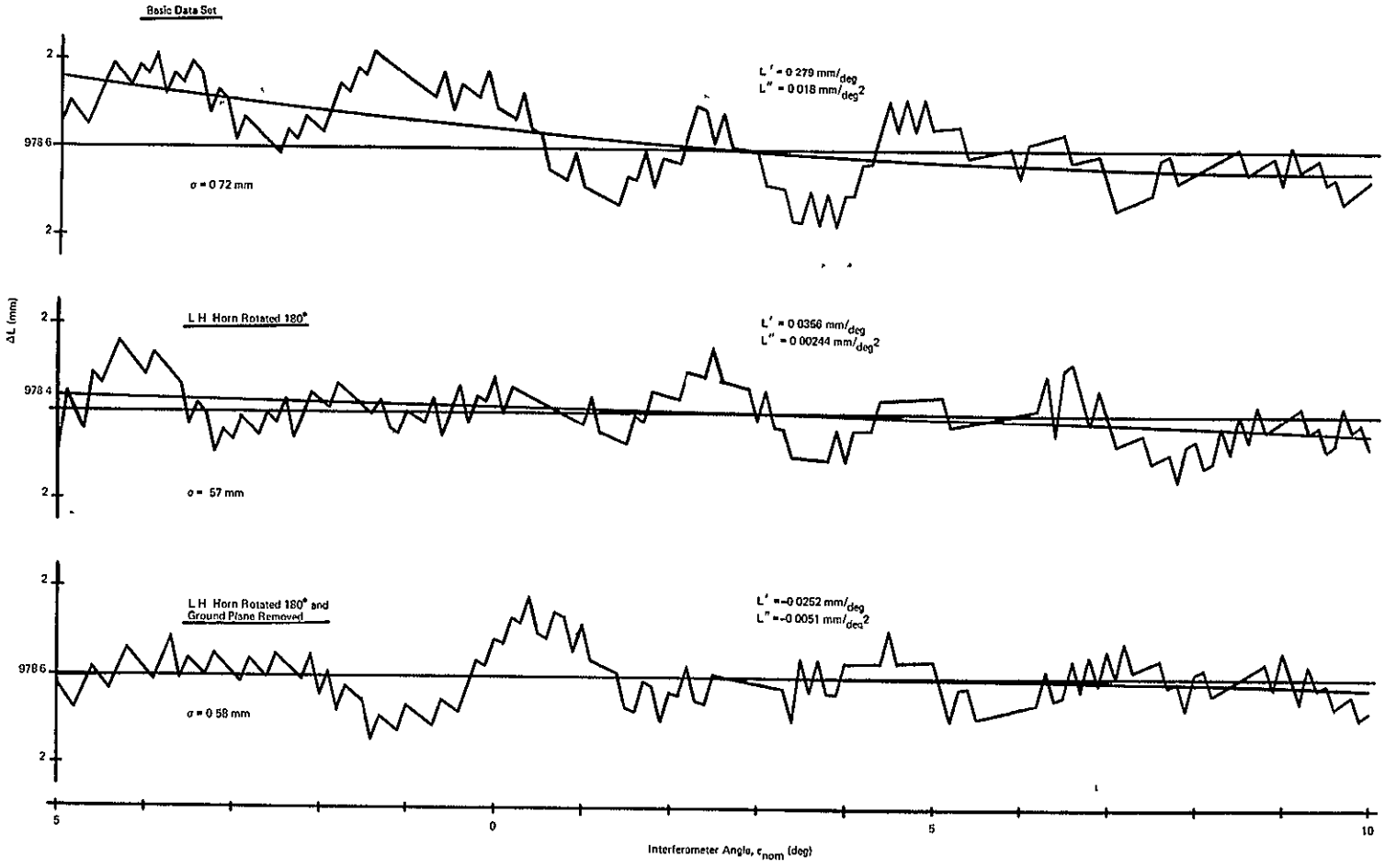

Figure 7-4. Estimated Baseline Length Using Two Illuminators

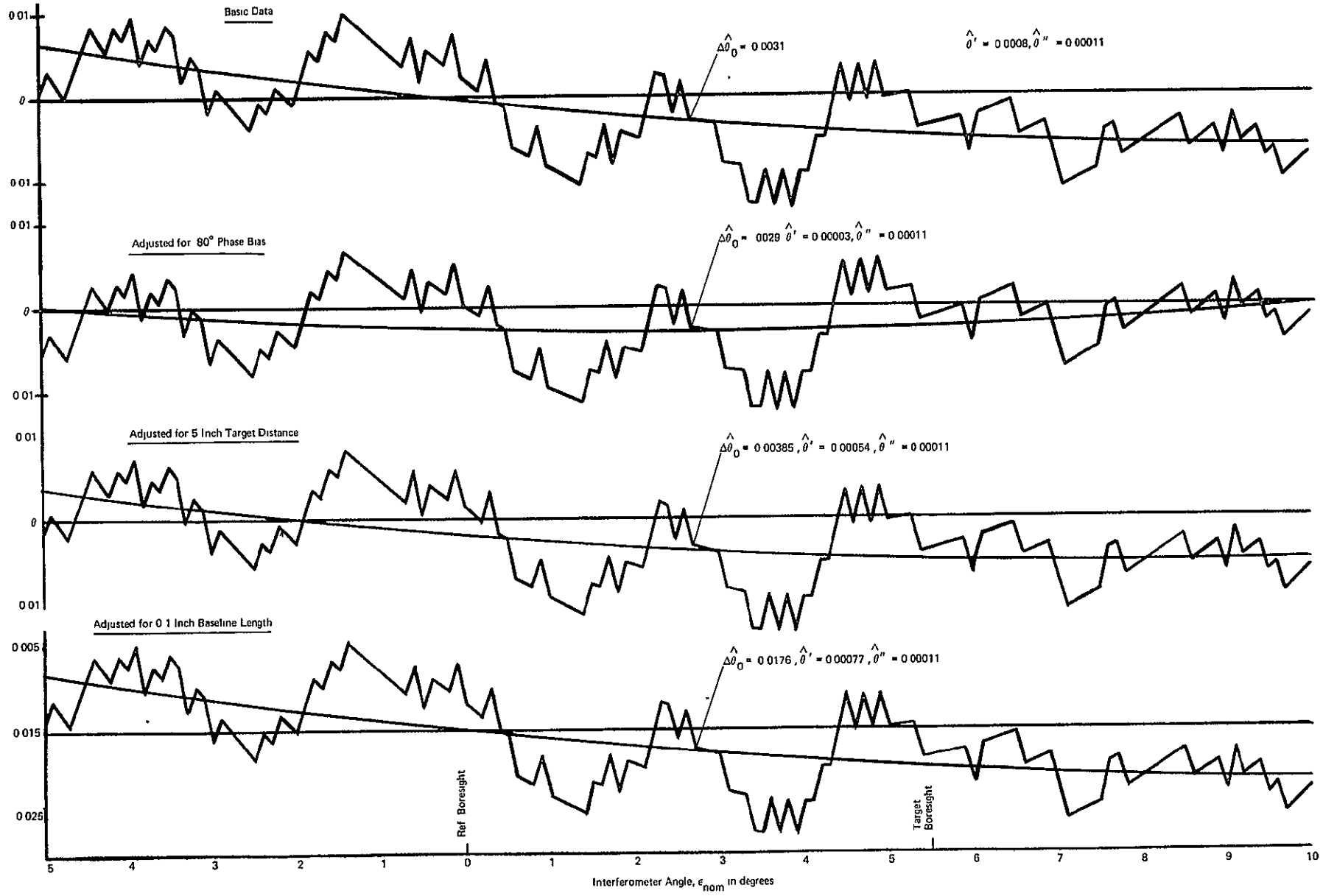

Figure 7-5. Experiment Data with Adjustements to Selected Parameters

less than 10 mm for a 400 λ baseline in order to achieve the 1 km position accuracy. No extrapolation of results from the 26.6λ to the 400 λ baselines is necessary since the phase center stability for the satellite application, at least, will be independent of the length of the baseline. As seen from Figure 7-4, the stability is five times better than required; and if the ground plane antenna interaction is the source of the slowly varying residuals, then the stability for a satellite application would be excellent.

In Figure 7-4, there is no significance to the ordinate in an absolute sense because it was arbitrarily chosen as the estimated value of L_V when the interferometer orientation was midway between the two illuminators. However, the variations within a data set and across the data sets are significant.

Notice that L_V appears to have shortened by 0.2 mm when the L. H. horn is rotated 180^o. The residuals also decreased significantly from σ = 0.72 mm to σ = 0.57 mm. Removing the ground plane appears to increase L_V by 0.2 mm without an attendant increase in σ.

7.4 EXPERIMENT DATA WITH ADJUSTMENTS TO SELECTED PARAMETERS

The basic data set was reprocessing three times, each time adjusting a different parameter.

The object was to demonstrate that the trends, i.e., $\Delta\theta_o$, θ', θ'' could be removed by proper adjustments to the parameters, i.e., the calibration process. Figure 7-5 gives the results. Analysis yielded the following equations:

$$\frac{\Delta\theta}{\Delta L_V} = \frac{1}{L_V}\left[-\theta\left(1+\frac{\theta^2}{3}\right)+\theta^2\epsilon-\theta\epsilon^2\right] \tag{7-1}$$

$$\frac{\Delta\theta}{\Delta\gamma_B} = \frac{\lambda}{2\pi L_V}\,\theta(\theta-2\epsilon). \tag{7-2}$$

Substituting into these equations the best estimates of the parameters yields

$$\frac{\Delta\theta\ (\text{deg})}{\Delta\ L_v(\text{mm})} = -0.0588 + 1.02 \times 10^{-5}\epsilon - 1.78 \times 10^{-6}\epsilon^2 \quad (\epsilon \text{ in deg.}) \tag{7-3}$$

$$\frac{\Delta\theta\,(\text{deg})}{\Delta\gamma_B(\text{deg})} = 5.85 \times 10^{-5} - 1.03 \times 10^{-5}\,\epsilon \quad (\epsilon \text{ in deg.}) \tag{7-4}$$

The basic data set shows $\theta' = 0.0008$. The value of $\Delta\gamma_B$ necessary to reduce θ' to zero is found from Equation (7-4):

$$\Delta\gamma_B \cong 80 \text{ deg.} \tag{7-5}$$

Therefore -80° of phase is subtracted from all data recorded for that set and reprocessed. The result is shown by the second curve of Figure 7-5. Notice that θ' has been reduced from 8×10^{-4} to 3×10^{-5}, whereas θ_o and θ'' remain essentially unchanged (which is in agreement with Equation 7-4).

If the baseline estimate were adjusted by +0.1 inches (2.54 mm), Equation (7-3) predicts that·

1. $\Delta\theta_o$ will change by -0.015 degree
2. θ' will change by +0.000026 degree
3. θ'' will change by -0.0000045 degree.

From Figure 7-5, the bottom curve, we see that

1. θ_o changed by -0.0145 degree
2. θ' changed by +0.00003 degree
3. θ'' changed by less than 0.00001 degree.

Notice the similiarity between the second and third data sets and the basic data data set adjusted for -80° of phase. Especially observe the effect on θ'.

Previously it was hypothesized that rotating the horn or removing the ground plane could change the phase center of the interferometer antennae. This shift in phase center can either be laterally, which effectively changes the baseline length, or axially, which would appear to cause a phase bias.

The RF wavelength was 1.45 inches (36.8 mm). Eighty degrees of phase at that wavelength corresponds to $\frac{80}{360}$ (1.45) = 0.321 inch (8.16 mm). Now if, for example, the L. H. horn phase center moved axially 0.321 inches relative to the R. H. horn the electrical baseline and a physical baseline (one that might be measured optically) orientation would differ by only $\Delta\epsilon = \frac{0.321}{38.5} = 8.33 \times 10^{-3}$ radians or 0.479 degree. By visual means (the only means available due to the limited funds) this difference would be imperceptible.

7.5 INDEPENDENT ANTENNA PHASE CENTER STABILITY INVESTIGATION

A short investigation was made to determine whether the slowly varying residuals could be caused by the difference in illumination angles at the two interferometer antenna, i.e., see β_{right} and β_{left} in Figure 7-1. If $\beta_{\text{right}} = \beta_{\text{left}}$ for all ϵ and the R. H. and L. H. antenna are near electrical duplicates, then the two antenna phase centers track and the individual phase center shifts are effectively canceled. Of course, if $\beta_{\text{right}} \neq \beta_{\text{left}}$ as ϵ changes, then even perfect duplicates of antennae cannot track. Figure 7-6 shows how the difference in illumination angle varies with ϵ. The average magnitude of the difference is much less important than how the difference changes with ϵ. The change with ϵ is less than 0.2 degree across the entire range of ϵ. Figure 7-7 shows the measured phase center characteristics for the two horns. The instability is expressed in degrees of phase which does not separate the lateral (baseline length variations) and radial (phase bias like variations) translations. However, assuming that the shift is first all lateral and then all radial coupled with the 0.2 degree $\Delta\beta$ difference could not explain the magnitude of the slow variations shown in Figures 7-3, 7-4 and 7-5.

7.6 SIMPLIFIED SPHERICAL WAVEFRONT INTERFEROMETER EQUATION

When the illuminating antennae are not at large distances from the interferometer, the math model which converts phase information into angle information becomes very complex as evidenced by Equation (7-5) where γ_s is the measured phase and ϵ is to be determined.

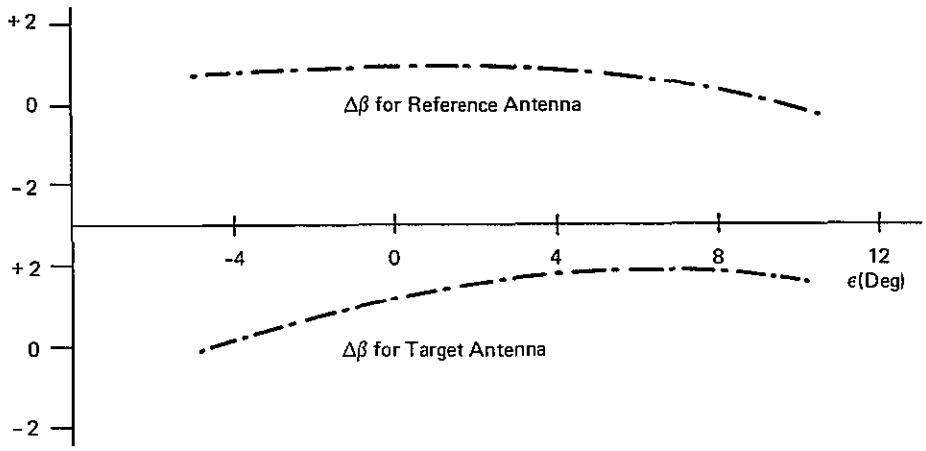

Figure 7-6. Variation in Illumination Angle for Interferometer Antennae vs. Orientation Angle ϵ

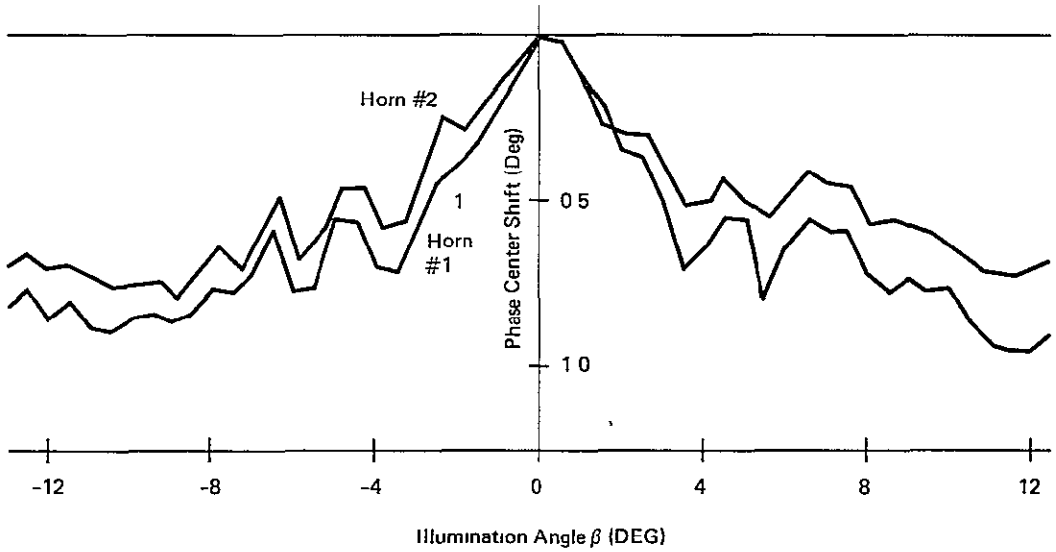

Figure 7-7. Variation in Antenna Phase Center with β, the Illumination Angle

It can readily be shown using series expansions that (7-5) can be expressed as

$$\gamma_s = \gamma_p (1 + C_1 + C_2 \gamma_p^2 + C_4 \gamma_p^4 + \ldots\ldots)$$

where

$$C_1 = -\frac{1}{8}\left(\frac{L_v}{d}\right)^2\left[1 - 3/16\left(\frac{L_v}{d}\right)^2 + 5/128\left(\frac{L_v}{d}\right)^4\right] \tag{7-6}$$

$$C_2 = \frac{1}{8}\left(\frac{\lambda}{2\pi d}\right)\left[1 - 5/8\left(\frac{L_v}{d}\right)^2\right].$$

Since $C_2 \ll 1$ and assuming $\gamma_s \approx \gamma_p$, a useful approximation of (7-6) is

$$\gamma_p = \frac{\gamma_s}{1 + C_1 + C_2\gamma_s^2} \tag{7-7}$$

Since C_1 and C_2 are constants, γ_p is readily computed. Value γ_s is the measured phase and γ_p is the equivalent plane wave phase.

The transformation from electrical phase to space angle can now assume the familiar form

$$\gamma_p = \frac{2\pi L_v}{\lambda} \sin(\theta - \epsilon). \tag{7-8}$$

The largest space angle error attributable to the interchange of γ_s and γ_p in Equation (7-7) is 2×10^{-5} degrees, assuming $L_v = 38.5$ inches and $d \approx 200$ inches.

Section 8

TOPICS IN TRADEOFF ANALYSIS

8.1 SYSTEM VARIABLES AFFECTING POSITION LOCATION ACCURACY

The major independent variables in an interferometer system for a particular application are the user ERP, frequency, baseline length, and transmission time or duration. These variables affect the phase errors and resulting position location error either directly or through dependent variables. Figure 8-1 illustrates the relationships in block diagram or signal flow form

To simplify the diagram, only phase errors due to thermal noise, instrumentation and multipath are shown. A later diagram will show the multipath interrelationships in more detail.

By use of such diagrams, the available tradeoffs in system design become clear, not only for location of balloons, but for other applications of interferometers as well. Some independent variables affect system characteristics or phase errors in addition to those mentioned above. For example, the frequency affects refraction error. The transmission duration affects multiple access or probability of interference of signals.

There are constraints in the dependent variables as well as the independent variables. Three of the contraints are:

1. Signal-to-noise ratio must be greater than (say) 10 dB in 50 Hz in order to limit the difficulty of signal acquisition.
2. The number of wavelengths of the baseline ($\frac{L}{\lambda}$) should be less than (say) 600 in order to limit the number of antennas and associated electronics required in the spacecraft for ambiguity resolution.
3. The boom twist should be less than (say) 10^{o} in order to limit errors due to polarization mismatch.

Some of the tradeoffs are discussed in the next sections.

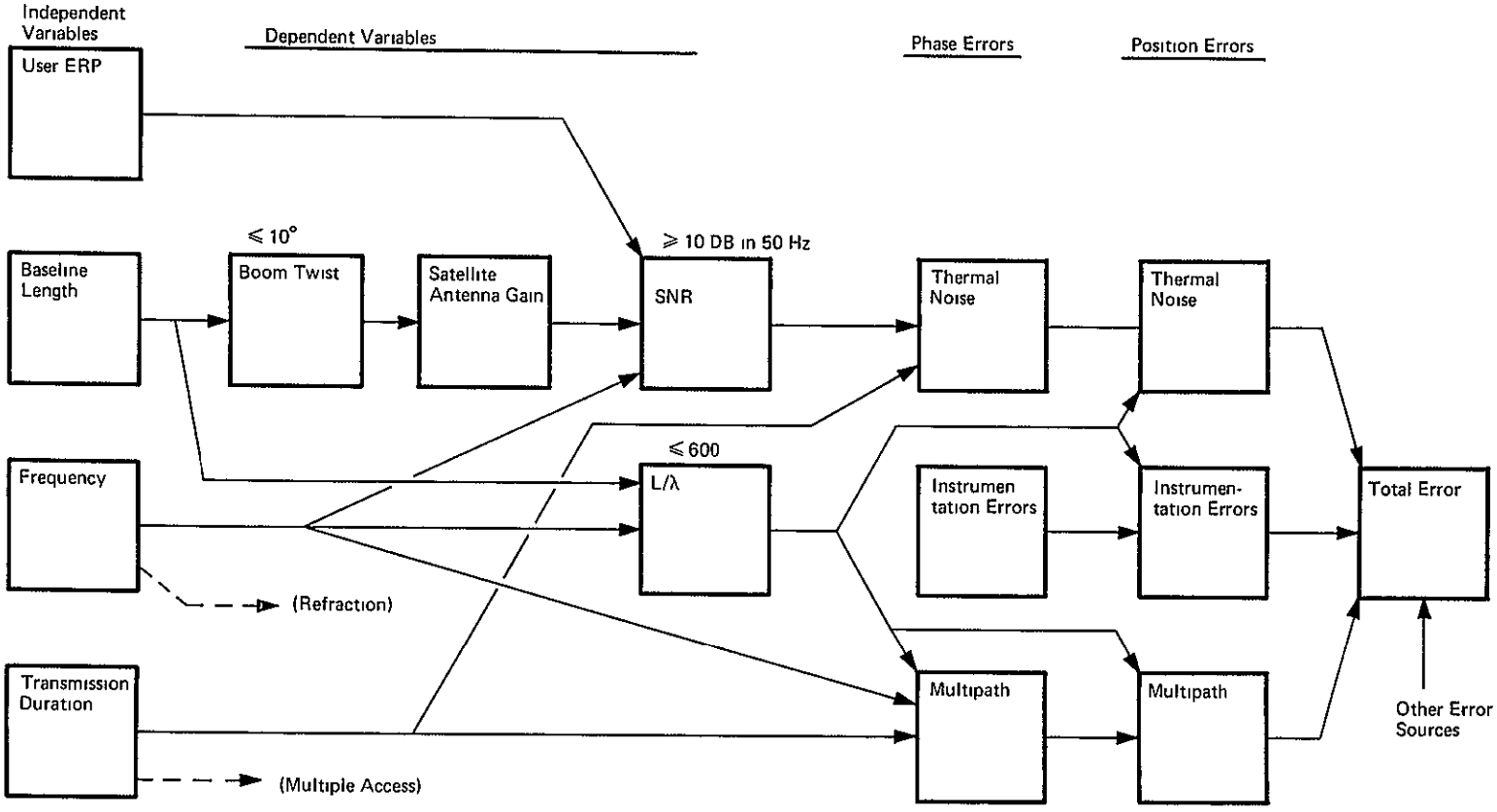

Figure 8-1. Variables Affecting Position Accuracy

8.2 TRADEOFF ANALYSIS OF BASELINE LENGTH AND SATELLITE ANTENNA GAIN

As indicated in Figure 8-1, the baseline length affects the position error via two mechanisms. First, the baseline length directly affects $\frac{L}{\lambda}$. Position errors due to fixed phase errors are inversely proportional to this parameter. Secondly, the amount of boom distortion which will occur is a function of boom length. The primary effect of boom distortion is the misalignment of the antennas at the boom ends. For both the extendible metal tape booms and the Astro column type boom, twisting of the boom due to nonuniform solar heating is the major cause of baseline distortion.

The major effect of boom twist is that permissible interferometer antenna gain is reduced, which is important for low power user applications. Other considerations are phase center tracking of antennas and phase errors due to polarization effects. The latter is the more sensitive of the two and will constrain the design to limit boom twist to something less than 10^{o}, depending upon choice of polarizations. If we restrict the problem to thermal noise errors, the question arises as to what boom length minimizes the position error due to this effect. To answer this question we must know the dependence of boom twist on length of boom. This dependence is a function of the boom type. Although some experimental data was taken in a thermal vacuum chamber on metal tape boom samples up to 10 feet long *, there is insufficient data at this point to verify the form of the dependence.

For illustrative purposes, we shall assume two forms of dependency:

1 Twist proportional to square of boom length, and

2. Twist proportional to boom length

*Discussions with personnel in Materials Research and Development Branch, Code 735, Goddard Space Flight Center.

First, assume

$$\Theta_t = bL^2 \tag{8-1}$$

where Θ_t = boom twist

b = constant

L = boom length

Then we shall make the antenna beamwidth equal to

$$\theta_b = 17.5^o + 2\theta_t \tag{8-2}$$

In order to have circular polarization, the antenna pattern will be symmetric about boresight so that the antenna gain will be

$$G_s = \frac{C_1}{(\theta_b)^2} \tag{8-3}$$

Then the signal-to-noise ratio received at the interferometer will be

$$SNR = C_2 G_s \tag{8-4}$$

$$= C_3 \theta_b^{-2}$$

where C_1, C_2 and C_3 are constants

The standard deviation of the termal noise error, σ_{th}, will be

$$\sigma_{th} = (SNR)^{-\frac{1}{2}} \tag{8-5}$$

$$= C_3^{\frac{1}{2}} \theta_b \tag{8-6}$$

and the standard deviation of the position error will be

$$\sigma_x = C_4 \frac{\lambda}{2\pi L} \sigma_{th} \tag{8-7}$$

where C_4 is a constant.

Using (8-2) and (8-5) this equation becomes

$$\sigma_x = \frac{C_5}{L}\left[17.5 + 2bL^2\right] \tag{8-8}$$

If σ_x is minimized with respect to the baseline, L, we find

$$L = \left[\frac{17.5}{2b}\right]^{\frac{1}{2}} \tag{8-9}$$

Under this condition the twist angle is, from (8-1),

$$\theta_t = 8.75^{\circ}.$$

The conclusions one can draw from the above are:

1. Minimum possible boom twist is desirable, and boom choice will strongly depend on this criteria.
2. For a given boom type, if boom twist is proportional to the square of boom length, position error due to thermal noise is minimized by using a boom length given by Equation (8-9). This can be considered an upper bound, i.e., there is no advantage to designing a system (in which thermal noise errors predominate) with a boom length exceeding the value given by Equation (8-9).

If the above analysis is performed with boom twist proportional to boom length, the result is that the position errors due to thermal noise are monotonically decreasing with boom length.

An alternate approach to determining antenna gain from that implied in Equation (8-2) is to consider the effect of boom twist on satellite antenna gain as a function of elevation angle of the user, as illustrated in Figure 8-2. Two values of antenna beamwidth (3 dB), 22 and 28 degrees are shown. For boom twist less than 6 degrees, the effective antenna gain is always larger with a satellite beamwidth of 22 degrees unless the elevation angle is less than 30 degrees.

For an interferometer in which boom twist will be less than 6 or 8 degrees, the optimum antenna beamwidth will be between 22 and 28 degrees.

8.3 MINIMIZING POSITION ERROR WITH RESPECT TO FREQUENCY

Figure 8-1 illustrates the major effects of frequency upon the system. Frequency, through the parameter L/λ, affects position errors due to all phase errors. Due to space loss, frequency affects the signal-to-noise ratio

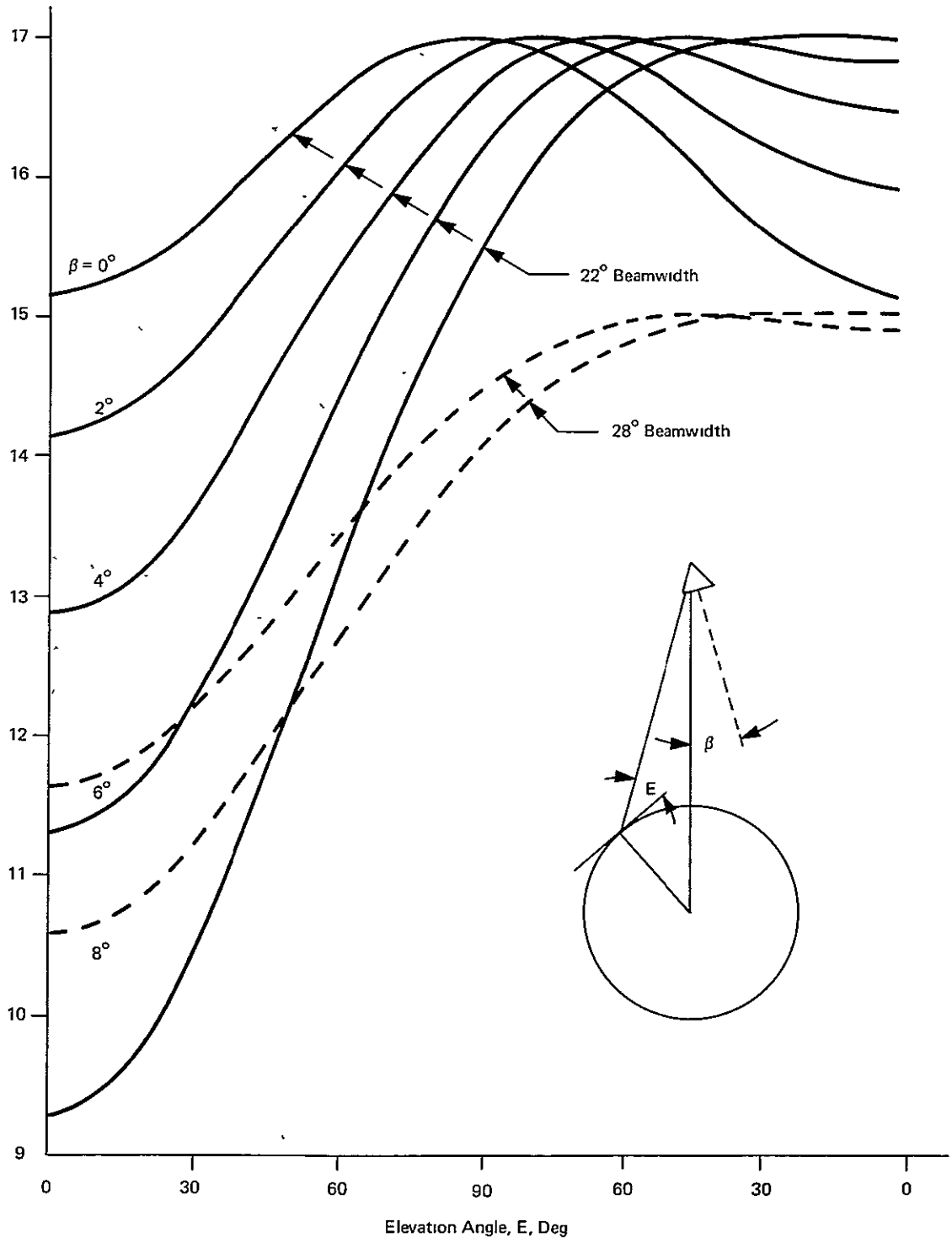

Figure 8-2. Effect of Boom Twist on Antenna Gain

and the resulting thermal noise phase error. In addition, it affects the multipath phase error, which will be discussed in subsection 8.4.

In the Final Report (Phase I) for this contract, it was shown that the error in position location due to thermal noise is independent of frequency for a given ERP. With this assumption it is desirable to use the highest frequency possible, consistent with other constraints, in order to minimize position errors due to instrumentation errors and multipath.

Another consideration in minimizing the costs of balloon packages is to minimize the DC power required. Using the DC power as one of the independent variables, we would obtain the diagram shown in Figure 8-3 to illustrate the relationships. As an approximation, in order to obtain a closed form solution, we shall assume that the effective radiated power for a given dc power is inversely proportional to the square root of the frequency. According to this assumption, twice as much ERP is available at 400 MHz as at 1600 MHz. The assumption can obviously be valid (even approximately) only over a limited frequency range. With this assumption, and assuming fixed gain antennas on the balloon and the interferometer, the received signal-to-noise is

$$SNR = \frac{C_5}{f^{2.5}} \tag{8-10}$$

where C_5 is a constant. The variance of the phase error, σ_ϕ^2, is then

$$\sigma_\phi^2 = \sigma_I^2 + \sigma_{th}^2 \tag{8-11}$$

where σ_I^2 = variance of instrumentation error

σ_{th}^2 = variance of phase error due to thermal noise.

The standard deviation of position error due to these two sources is

$$\sigma_x = C_6 \left(\frac{\lambda}{L}\right) \sigma_\phi \tag{8-12}$$

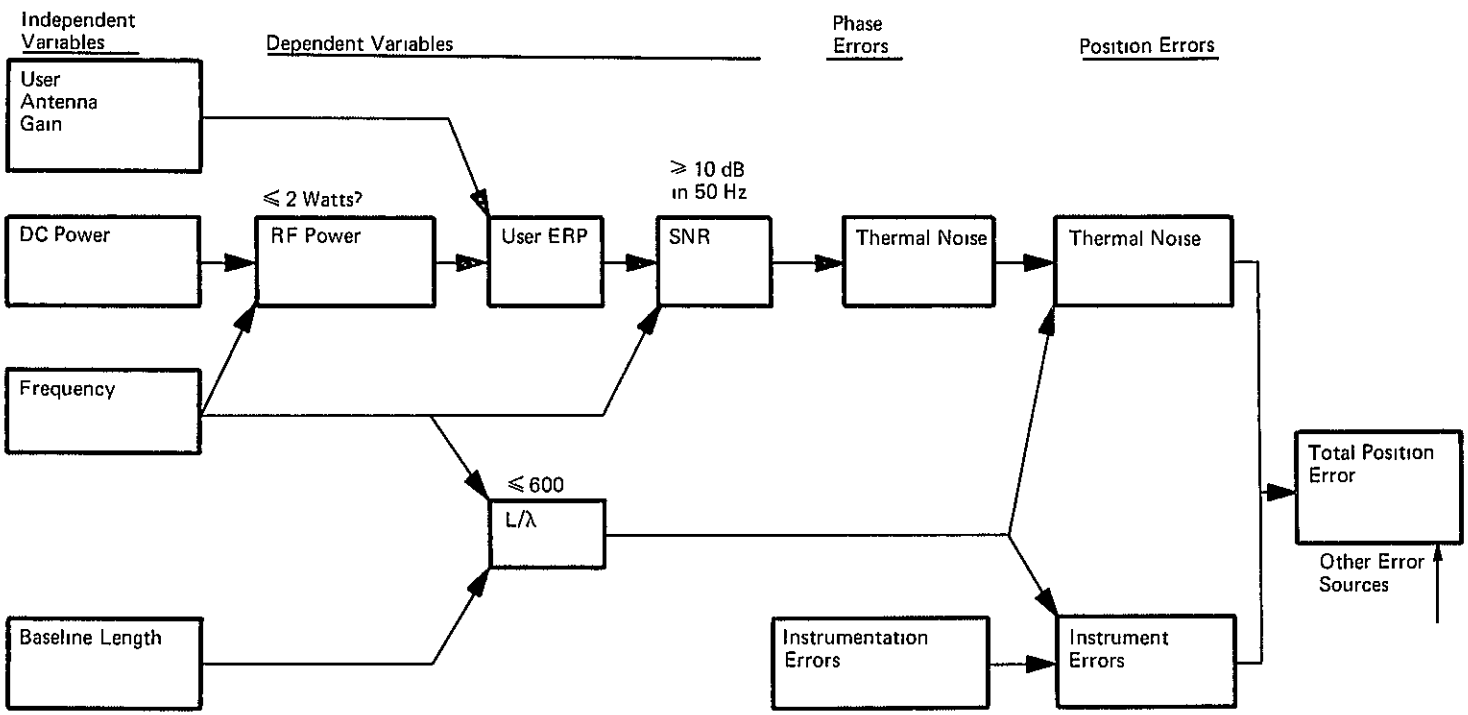

Figure 8-3. Relationship with DC Power as Independent Variable

and using (8-5) and (8-4), Equation (8-12) becomes

$$\sigma_x = \frac{C_7}{f}\left[\sigma_I^2 + \frac{f^{\frac{5}{2}}}{C_5}\right]^{\frac{1}{2}} \quad . \tag{8-13}$$

This expression is minimized with respect to frequency when

$$f_{opt} = \left[4\sigma_I^2 \; C_5\right]^{\frac{2}{5}} \quad . \tag{8-14}$$

At this frequency, from equations (8-5) and (8-10), we have

$$\sigma_{th} = 2\,\sigma_I \quad . \tag{8-15}$$

From this we can conclude the following:

> To minimize position error due to thermal noise and instrumentation errors for a given DC power in the emitter (and assuming a $f^{-0.5}$ dependence of ERP), the optimum frequency is that value where the thermal noise phase error is twice the instrumentation phase error.

The sensitivity of the resulting error to operation at other than the optimum frequency is important. By using a frequency h times the value given by equation (8-14), or

$$f = h\, f_{opt} \tag{8-16}$$

we find:

$$\sigma_x = \sigma_x\,(opt)\left[\frac{1+4h^{2.5}}{5h^2}\right]^{\frac{1}{2}} \tag{8-17}$$

where σ_x (opt) is that value given by Equation (8-13) for the optimum frequency. For frequency twice or one-half of the optimum (h = 2 or 1/2), the resulting position error would be 1.086 or 1.13, respectively, times the optimum. Therefore, σ_x minimum is not a strong function of frequency near the optimum.

If we are working at the optimum point and the instrumentation error were actually double what we expected it to be, the position error would increase to 1.26 times the "optimum." If the thermal noise error would double from the expected value, the position error would increase to 1.84 times the "optimum."

8.4 VARIABLES AFFECTING POSITION ERRORS DUE TO MULTIPATH

The interferometer variables which affect performance due to multipath are baseline length, frequency, and antenna polarization. The other characteristics pertaining to the system are the user antenna polarization and transmission duration. Other variables which affect the multipath performance are user antenna gain characteristics, location, altitude and velocity. These, of course, depend upon the application. The relationships are illustrated in Figure 8-4.

As can be seen, the dependent variables of importance are L/λ, reflection coefficient, per unit reflected power, whether the multipath reflection is diffuse or specular, and the amount of bandspreading (if scattering is diffuse). Then, effective signal-to-multipath ratio, with the correlation of phase errors across the baseline (determined by L/λ , and user location and altitude), will determine the phase error across the baseline and the resulting position error due to multipath.

Details of the relationships above are derived in the Final Report (Phase I)[1] Figure 8-4 displays cause-effect relationships among the variables, in order to bring into focus the tradeoffs available for different applications of a position location interferometer.

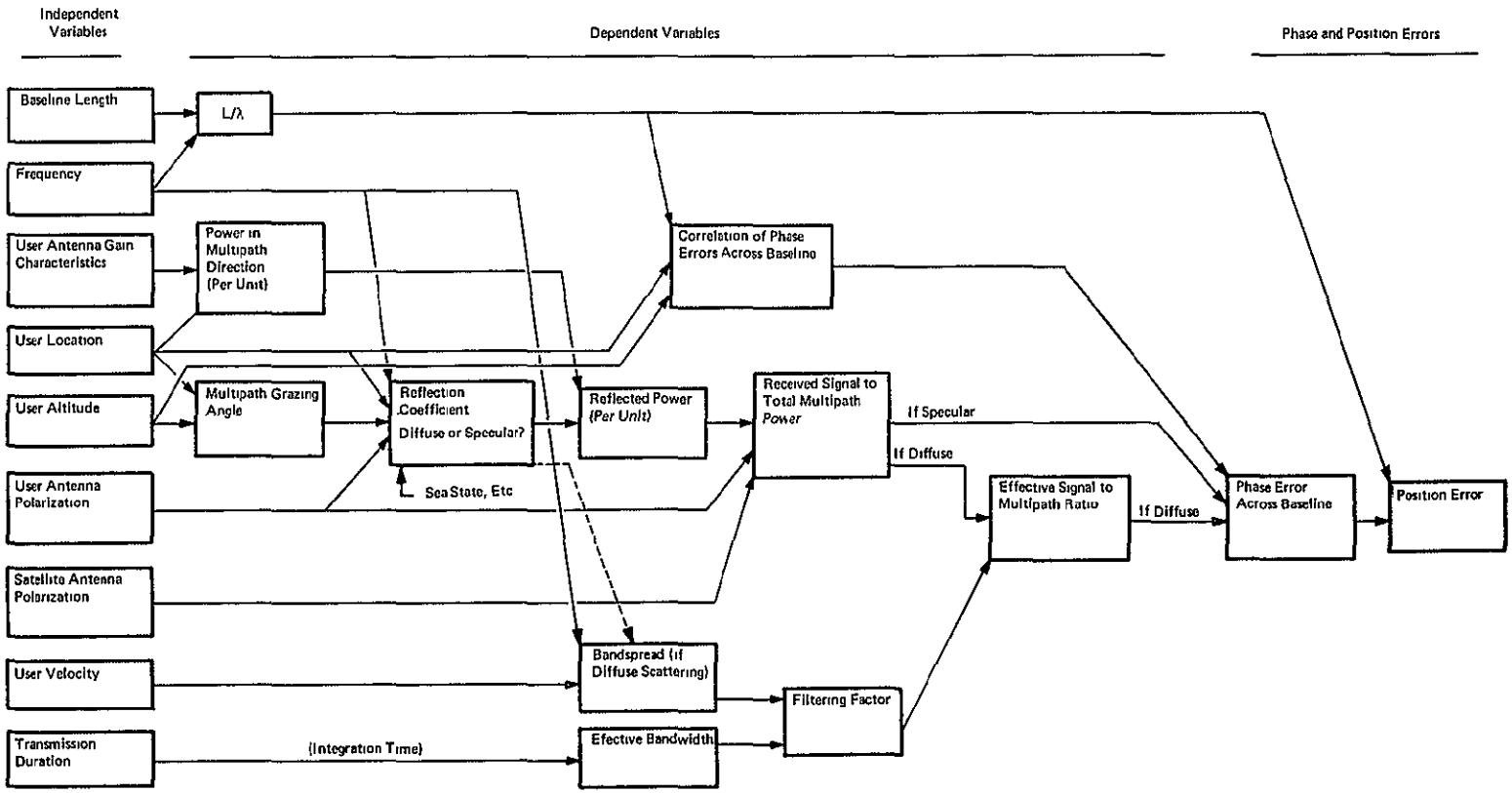

Figure 8-4. Relationship of Variables Affecting Multipath Position Error

Appendix

DESCRIPTION OF ATS F&G BREADBOARD INTERFEROMETER

The breadboard interferometer is a precision, wide field-of-view attitude sensor. It determines attitude angles by measuring phase differences between pairs of antenna elements induced by the incoming RF signal. The interferometer consists of one vernier (26 6 wavelengths) and one coarse (1.6 wavelengths) baseline. The latter resolves the ambiguities inherent in the vernier baseline.

The system utilizes and RF-switched dual-channel receiver, frequency multiplexing prior to detection, and a digital phase measurement technique. Critical parameters are the phase tracking of the system components and the phase center stability of the antenna elements. Accurate alignment techniques utilizing optical techniques have been developed and successfuly implemented. The system is designed to meet a 3-sigma, 0.03-degree (spatial angle) accuracy over a field of view of at least +17.5 degrees with a resolution of 0.004 degrees. A more detailed description of the breadboard model follows.

Figure A-1 is the interferometer breadboard block diagram. The receiver is a switched dual-channel, triple down-conversion system using a direct digital counting technique. The vernier and coarse antenna elements are switched by a solid-state switch.

Two 8.155 GHz RF signals from two antenna elements (either Ref/vernier or Ref/coarse) with phase information are fed into the first mixers, where they are down-converted to 155 MHz and amplified while preserving phase information. These two signals are again down-converted to a pair of signals to 32.5 MHz spaced 2 kHz apart by using the double local oscillator. This pair of signals is then summed, amplified, and detected. The 2 kHz difference frequency is then phase-compared with the 2 kHz reference signal which was used to phase-lock the double local oscillator.

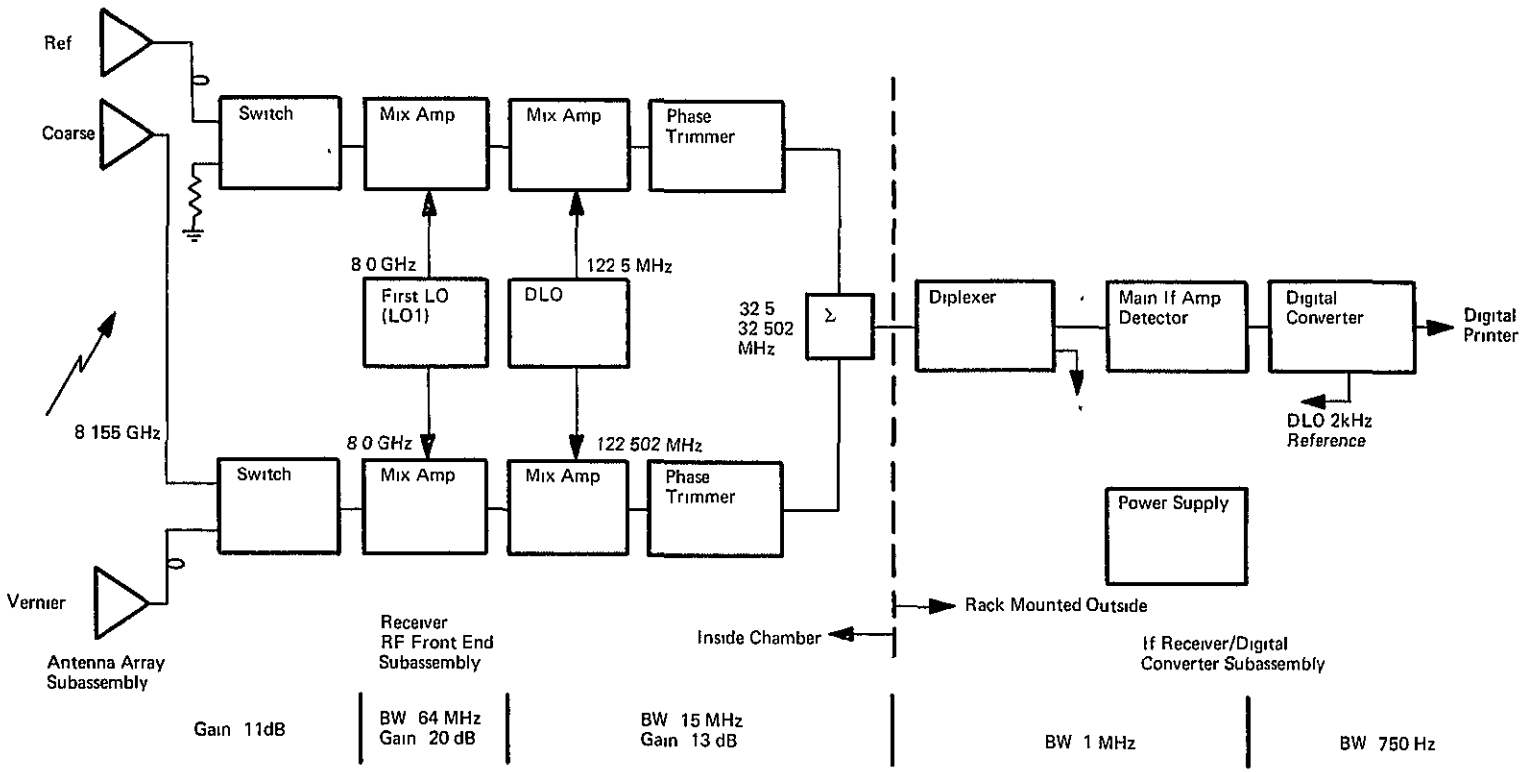

Figure A-1. ATS F&G Breadboard Interferometer Block Diagram

The digital converter (phase meter) converts the phase difference between the detected 2 kHz from the incoming signals and the 2 kHz reference signal into digital counts by using one to gate a counter on and the other to gate off. To reduce the phase jitter caused by random noise, 64 successive counts are averaged together.

A.1 SUBASSEMBLY DESCRIPTION

The breadboard interferometer consists of three major subassemblies:

1. Antenna array including waveguide-to-coaxial transitions and coaxial cables
2. RF components including dual-channel receiver and summing network
3. Main IF/detector and digital converter.

The array and RF components are installed inside the anechoic chamber in which the system tests are conducted. The main IF/detector and digital converter are rack-mounted outside the chamber.

A.2 ARRAY ASSEMBLY

The array assembly consists of

1. Three antenna elements
2. Three transmission lines
3. One baseline and support structure
4. One ground plane.

The antenna element is an amplitude-compensated pyramidal horn with longitudinal plates inserted along the horn axis perpendicular to the electric field. The E-plane sidelobe levels are better than 25 dB below the main lobe, and the -3 dB beamwidths in both the E- and H-planes are equal to 40°. The VSWR of the horn is typically less than 1.1 and the gain is 13 dBI. The horns were made by the aluminum dip brazing process with mechanical tolerances held closely in order to provide good mechanical symmetry and hence good phase tracking between antennas. The measured phase tracking between the

antennas in both the E and H planes was +0.25 electrical degree over a spatial field of view of ±20 degrees.

The antennas are fed by an X-band waveguide-to-coaxial line adapter which mates with the transmission line. The transmission line is 0.141 inch diameter semi-rigid cable with miniature connectors. Techniques have been developed that provide phase-balanced sets of transmission lines that can track to within ±0.25 electrical degree over a temperature range of 0 to 50°C.

A.3 RF FRONT END ASSEMBLY

The RF front end is a dual-channel, double-conversion receiver consisting of the following off-the-shelf components:

1. A pair of HP solid-state SPDT (33006A)
2. A pair of isolators (221-0815, Addington Laboratory)
3. A pair of first mixer/amplifiers (LEL XMC-7-8654)
4. First LO (ATI)
5. A pair of Relcom second mixers
6. Dual LO (Frequency Electronics)
7. A pair of Ampar IF amplifiers (LN4-22G-10)
8. A pair of phase trimmers (Merrimac PS-3)
9. A summing network Iso-T (TV-50).

The solid-state switches have been selected for arm-to-arm phase balance within ±2 electrical degrees. They are designed for broadband applications and consist of PIN diodes in a hermetically sealed stripline package. Typical measured parameters are:

VSWR:	1.15
Isolation:	>60 dB (arm-to-arm)
Insertion loss:	1.1 dB
Phase balance:	±1.5°

The isolators consist of circulators with internal terminations. They are placed at the input to the first mixer amplifiers in order to reduce the LO radiation through the antennas. They exhibit typical isolation in excess of 40 dB with a VSWR of 1.04 and an insertion loss of 0.5 dB.

The first mixer/amplifier converts the RF signal to a 155 MHz signal. It consists of a pair of matched diodes and two transistor amplifier stages. It provides 19 dB gain with a 10.5 dB noise figure for a -3 dB bandwidth of 64 MHz.

The first local oscillator consists of a crystal-controlled multiplier chain with dual outputs to the mixers. It varies less than +100 kHz from the nominal frequency of 8 GHz over a temperature range of 0 to 50°C. All harmonics and spurious signals are more than 60 dB below the desired signal. The two output ports are amplitude-balanced to within 0.2 dB and phase-balanced to within 0.5 electrical degree over the temperature range of 0 to 50°C.

The second mixer is a wideband bridge type miniature design. It exhibits a 7 dB conversion loss. The relative phase shift of a pair of mixers versus RF input signal level (-10 to -50 dBm) is negligible. The second amplifier is a low noise transistor amplifier with a gain of 20 dB, a noise figure of 3 dB and a bandwidth of 15 MHz.

The dual local oscillator (DLO) provides two LO signals at 122.500 and 122.502 MHz to the second mixers. The 2 kHz offset is obtained through a phase-locked loop with the loop frequency of 2 kHz slaved to the 2 kHz reference clock. The frequency stability after warmup is 0.2 ppm/hr. Phase stability is one of the most important characteristics of this unit. The relative phase of interest is between the 2 kHz reference supplied to the DLO and the 2 kHz flat note at the RF outputs. The total change of this phase is less than 1.8 electrical degrees over a temperature range of 0° to 50°C.

A.4 IF RECEIVER AND DIGITAL CONVERTER ASSEMBLY

The IF receiver is designed to receive a pair of CW signals (spaced 2 kHz apart) from the summing network and to process this pair of signals so that

the output is a 2 kHz sine wave whose phase relative to the digital converter 2 kHz reference is independent of signal input level and nominal changes in input signal frequency.

The receiver consists of six transistor stages, a square low detector, AGC loop, a bandpass filter (fo = 2 kHz, BW = 750 Hz) and a 3 stage buffer amplifier. The 2 kHz sine wave output is fed into a zero crossing detector.

The 2 kHz sinusoidal signal is converted into a square wave using a sensitive zero-crossing detector. The 2 kHz signal is phase-compared with the 2 kHz reference. The vernier or coarse signal can register up to 511 actual counts, but the number of possible values is 512, including zero. The vernier data (64 samples) is averaged to reduce the gating error by a factor of 8. Averaging, however, presents problems at discontinuities where the electrical phase due to noise is changing from 0 to 2π or vice versa. Such an error will not be experienced in a noiseless system. In a practical system with inherent noise, the representative samples would likely run as follows: 511, 512, 0, 0, 511, 1, etc. For gaussian noise with zero mean, this average would tend to be 256 counts, corresponding to an electrical phase of 180 degrees. To eliminate this problem in the vicinity of zero degrees, a discontinuity detector which detects a region about the discontinuities is implemented. A +16 count corridor about zero count is provided. If a preliminary sample reveals that the upcoming measurement is in the area near a discontinuity, the reference signal setting one side of the phase flip-flop is shifted 180 degrees (complemented) for that measurement. This is equivalent to subtracting 256 counts for a deviation to the right of the discontinuity and adding 256 counts for a deviation to the left of the discontinuity. When the reference signal is complemented, the last stage of the counter is also complemented, automatically adding or subtracting the 256 counts that were subtracted or added, respectively, when the reference signal was complemented. When the detector logic shows that the measurement is not in the area near a discontinuity, neither the reference signal nor the last stage of the counter is complemented. In addition, voting logic is implemented to reduce gross or impulse error in the preliminary

measurement. Three preliminary measurements are used instead of one. If at least two of three preliminary measurements indicate that the measurements are in the vicinity of zero count, the reference and last bit of count will be complemented.

Two registers are also incorporated in the system, one corresponding to parallel output and the other to serial output. The first register is isolated from the serializing register, and the readout from the serial register is not affected by the data dumped into the first register. Dual in-line integrated circuits, TI74N series, are used on seven basic cards.

In addition, four printer interface cards are mounted in the bracket with digital converter cards. The printer interface logic is, in effect, a 13-bit binary-to-BCD (1224 code) converter, and it can function independently of the digital converter. Likewise, the digital converter can function independently of the printer interface logic. Implementation of printer interfacing with the digital converter is provided only for ease of breadboard system test, i.e., to print out count vs space angle directly.

The measurements performed on the interferometer indicate that it has an accuracy of +0.004 space angle degrees. The tests indicate that this accuracy is maintained over a 30 dB dynamic range, and for signal frequency variation of $\pm$100 kHz.

REFERENCES

1. Interferometer Position Location Concept, Final Report, IBM Report FSC 70-5193 prepared for Goddard Space Flight Center/NASA under Contract NAS 5-21043, June 1970.
2. World Weather Watch Planning Report No. 18, "The Role of Meteorological Satellities in the World Weather Watch," Secretariat of the World Meteorological Organization, Geneva, Switzerland, 1967.
3. Breadboard Test Data Report for Interferometer Subsystem, Fairchild Hiller/IBM, Contract NAS 5-11906, October 17, 1969.
4. Evincive Test Report, Interferometer Subsystem for ATS F&G, Fairchild Hiller/IBM, Contract NAS 5-11609, October 17, 1969.
5. Interferometer Subsystem, Proposal for ATS F&G (Phase D), Volume 1K, Fairchild Hiller/IBM, prepared under Contract NAS 5-11609, September 17, 1969.
6. Viterbi, A.J., Principles of Coherent Communications, McGraw-Hill, 1966, p. 36.
7. Sallen, R.P., and Key, E.L., "A Practical Method of Designing RC Active Filters," IRE Trans. Circuit Theory, Vol. CT-2, March 1955, pp. 74-85.
8. Two, J., "A Step-by-Step Active Filter Design," IEEE Spectrum, December 1969, pp. 64-68.
9. Geffee, Philip R., "Toward High Stability in Active Filters," IEEE Spectrum, pp. 63-66, May 1970.
10. Handbook of Universal Active Filter Use, Kinetic Technology, Inc.